

1
2
3 **Clinical Factors Associated with Microstructural Connectome Related Brain**
4 **Dysmaturation in Term Neonates with Congenital Heart Disease**
5

6 Jodie K. Votava-Smith^{†1}, Jenna Gaesser^{†2}, Anna Lonyai Harbison^{†3}, Vince Lee^{4,5},
7 Nhu Tran⁶, Vidya Rajagopalan⁷, Sylvia del Castillo⁸, Ram Kumar Subramanian⁹,
8 Elizabeth Herrup¹⁰, Tracy Baust¹⁰, Jennifer A. Johnson¹¹, George C. Gabriel¹²,
9 William T. Reynolds III⁴, Julia Wallace⁴, Benjamin Meyers⁴, Rafael Ceschin^{4,13},
10 Cecilia W. Lo¹², Vanessa J. Schmithorst⁴, and Ashok Panigrahy^{*4,5,13}
11

12 [†]*These authors have contributed equally to this work and share first authorship*
13 **Corresponding author*
14

15 ¹Division of Cardiology, Department of Pediatrics, Children's Hospital Los Angeles and
16 Keck School of Medicine of USC, Los Angeles, CA
17

18 ²Department of Neurology, Children's Hospital of Pittsburgh of UPMC and University of
19 Pittsburgh School of Medicine
20

21 ³Stanford Children's Health, Palo Alto, CA
22

23 ⁴Department of Pediatric Radiology, Children's Hospital of Pittsburgh of UPMC and
24 University of Pittsburgh School of Medicine
25

26 ⁵Department of Bioengineering, Swanson School of Engineering, University of
27 Pittsburgh
28

29 ⁶Fetal and Neonatal Institute, Division of Neonatology, Children's Hospital Los Angeles,
30 Department of Pediatrics, Keck School of Medicine of USC, Los Angeles, CA
31

32 ⁷Department of Radiology, Children's Hospital Los Angeles and Keck School of
33 Medicine of USC, Los Angeles, CA
34

35 ⁸Department of Anesthesiology Critical Care Medicine Anesthesiology, Children's
36 Hospital Los Angeles and Keck School of Medicine of USC, Los Angeles, CA
37

38 ⁹Division of Cardiothoracic Surgery, Department of Surgery, Children's Hospital Los
39 Angeles and Keck School of Medicine of USC, Los Angeles, CA
40

41 ¹⁰Pediatric Cardiac Intensive Care Division, Department of Critical Care, University of
42 Pittsburgh School of Medicine, Pittsburgh, PA
43

44 ¹¹Division of Pediatric Cardiology, Department of Pediatrics, University of Pittsburgh
45 School of Medicine, Pittsburgh, PA.
46

47 ¹²Department of Developmental Biology, University of Pittsburgh, Pittsburgh, PA

48

49 ¹³Department of Biomedical Informatics, University of Pittsburgh, Pittsburgh, PA

50

51

52 **Corresponding author:** Ashok Panigrahy, MD, Department of Pediatric Radiology,
53 Children's Hospital of Pittsburgh of UPMC, 45th Street and Penn Avenue, Pittsburgh PA
54 15201. Email: panigrahya@upmc.edu, Phone: 412-692-5510, Fax: 412-692-6929

55

56 **Funding:** This work was supported by the Department of Defense (W81XWH-16-1-0613),
57 the National Heart, Lung and Blood Institute (R01 HL152740-1, R01 HL128818-05), and the
58 National Heart, Lung and Blood Institute with National Institute on Aging (R01HL128818-05
59 S1). Southern California Clinical and Translational Sciences Institute (NCATS) through Grant
60 UL1TR0001855. Its contents are solely the responsibility of the authors and do not
61 necessarily represent the official views of the NIH. We also acknowledge Additional Ventures
62 for support (AP, VR, RC) VR is supported by the Saban Research Institute, Additional
63 Ventures Foundation and NIH-NHLBI K01HL153942.

64 Number of Tables: 4 main, 2 supplemental

65 Number of Figure: 5

66 Word Count: 8,742

67

68 Keywords: congenital heart disease, diffusion tensor imaging, connectome analysis, seed-based
69 tractography, subcortical brain dysmaturation, magnetic resonance imaging, clinical factors

70

71 **ABSTRACT:**

72 Objective: Term congenital heart disease (CHD) neonates display abnormalities of brain
73 structure and maturation, which are possibly related to underlying patient factors and
74 perioperative insults. Our primary goal was to delineate associations between clinical factors and
75 postnatal brain microstructure in term CHD neonates using diffusion tensor imaging (DTI)
76 magnetic resonance (MR) acquisition combined with complementary data-driven connectome
77 and seed-based tractography quantitative analysis. Our secondary goal was to delineate
78 associations between mild dysplastic structural abnormalities and connectome and seed-base
79 tractography as our primary goal.

80

81 Methods: Neonates undergoing cardiac surgery for CHD were prospectively recruited from two
82 large centers. Both pre- and postoperative magnetic resonance (MR) brain scans were obtained.
83 DTI in 42 directions was segmented to 90 regions using neonatal brain template and three
84 weighted methods. Seed- based tractography was performed in parallel. Clinical data :18 patient-
85 specific and 9 preoperative variables associated with preoperative scan and 6 intraoperative and
86 12 postoperative variables associated with postoperative scan. A composite Brain Dysplasia
87 Score (BDS) was created including cerebellar, olfactory bulbs, and hippocampus abnormalities.
88 The outcomes included (1) connectome metrics: cost and global/nodal efficiency (2) seed-based
89 tractography: fractional anisotropy. Statistics: multiple regression with false discovery rate
90 correction (FDR).

91

92 Results: A total of 133 term neonates with complex CHD were prospectively enrolled and 110
93 had analyzable DTI. Multiple patient-specific factors including d-transposition of the great
94 arteries physiology and severity of impairment of fetal cerebral substrate delivery were
95 predictive of preoperative reduced cost ($p < 0.0073$), reduced global/nodal efficiency ($p < 0.03$).
96 Multiple postoperative factors (extracorporeal membrane oxygenation [ECMO], seizures,
97 cardiopulmonary resuscitation) were predictive of postoperative reduced cost, reduced
98 global/nodal efficiency ($p < 0.05$). All three subcortical structures of the BDS (including
99 olfactory bulb/sulcus, cerebellum, and hippocampus) predicted distinct patterns of altered nodal
100 efficiency ($p < 0.05$).

101

102 Conclusion: Patient-specific and postoperative clinical factors were most predictive of diffuse
103 postnatal microstructural dysmaturation in term CHD neonates. In contrast, subcortical
104 components of a structurally based- brain dysplasia score, predicted more regional based
105 postnatal microstructural differences. Collectively, these findings suggest that brain DTI
106 connectome may facilitate deciphering the mechanistic relative contribution of clinical and
107 genetic risk factors related to poor neurodevelopmental outcomes in CHD.

108

109

110 **BACKGROUND:**

111 Congenital heart disease (CHD) is the most prevalent birth defect, accounting for nearly
112 one third of all major congenital anomalies.¹ While surgical techniques have vastly improved
113 survival in the past few decades, with most children with complex CHD now living to adulthood,
114 neurodevelopmental impairments have emerged as one of the most common long-term sequelae
115 of CHD survivors, including the realms of cognition, memory, social interaction, communication
116 and language, attention, and executive function.²⁻⁷ Neonates with CHD display findings of brain
117 dysmaturation as well as vulnerability to brain injury, assessed by magnetic resonance imaging
118 (MRI).⁸⁻¹⁰ The cause of the widespread neurodevelopmental delays seen in CHD children are
119 likely multifactorial, stemming from prenatal, genetic, and postnatal factors. Abnormalities of
120 brain growth and microstructure in CHD have fetal origins^{11,12}, and may result from impaired
121 oxygen and substrate delivery to the developing brain based on alterations of fetoplacental
122 circulation related to the CHD.¹³ Neurodevelopmental impairments in the CHD population
123 correlate more with brain immaturity rather than injury.^{14,15} Therefore, the traditional “lesion-
124 based approach” to specific brain injuries driving the widespread cognitive dysfunction seen in
125 CHD seems to fall short.

126 A brain connectome approach has emerged in recent years as a new paradigm to
127 understand the complexity of functional neural networks and how they influence human
128 behavior. This type of analysis has also been used to evaluate adolescents with d-transposition of
129 the great arteries (d-TGA), in which network topology differences were found to mediate
130 multiple domains of adverse neurocognitive outcomes.¹⁶ We have recently described a
131 quantitative data-driven network topology (connectome) graph analysis to compare neonates
132 with CHD to normal controls, and demonstrated the early presence of brain reorganization in
133 CHD neonates¹⁷⁻²¹. Other recent studies have described aberrant diffusion tensor -based
134 connectome in CHD neonates and infants in both preoperative and postoperative periods, finding
135 distinct patterns of structural network topology alterations¹⁷⁻²¹. There is also recent literature to
136 suggest that genetic factors might impact the structural connectome in CHD¹⁹. While the
137 connectome technique is a robust analytical tool, there are other hypothesis-driven approaches
138 that have been applied to quantifying diffusion tensor-based data in CHD which includes seed-
139 based tractography that facilitates quantitative metrics of cortical association tracts. Of note, pre-
140 clinical surgical based animal models of CHD show that the postnatal subventricular zone is
141 vulnerable to neurotoxicity from volatile anesthetic agents^{22,23} and hypoxia, resulting in diffuse
142 white matter injury (WMI) of white matter tracts, including the superior longitudinal fasciculus
143 (SLF), inferior longitudinal fasciculus (ILF) and fronto-occipital fasciculus (FOF), assessed by
144 diffusion tensor imaging (DTI) tractography techniques. Diffuse WMI also correlates with
145 cortical long-range connectivity dysmaturation. In contrast, focal WMI, acquired in CHD infants
146 on serial preoperative/immediate postoperative brain MRIs (usually performed on 7-14 postnatal
147 days and are detected with 3D-T1 based MR imaging), involve punctate periventricular fronto-
148 parietal white matter lesions involving long-range connectivity crossing-fibers,^{14,24-29} also caused
149 by hypoxia/inflammation.

150 A recent published study comparing critical/serious CHD prior to surgery and 116
151 matched healthy controls as part of the developing Human Connectome Project imaged with
152 high angular resolution diffusion MRI (HARDI) and processed with multi-tissue constrained
153 spherical deconvolution, anatomically constrained probabilistic tractography (ACT) and
154 spherical-deconvolution informed filtering of tractograms (SIFT2) was used to construct
155 weighted structural networks, and identified one subnetwork with reduced structural connectivity

156 in CHD infants involving basal ganglia, amygdala, hippocampus, and the cerebellar vermis^{17,18}.
157 We have recently described a similar pattern of structural subcortical dysmaturation both in
158 human infants with CHD and genetically relevant ciliary motion dysfunction, and also in relation
159 to preclinical models of CHD including hypoplastic left heart syndrome (HLHS).^{10,30-35} This
160 pattern of subcortical dysmaturation was predominantly seen in the olfactory bulb
161 (dysmorphometry of left and right olfactory bulbs and sulci), the cerebellum (hypoplasia and/or
162 dysplasia in cerebellar hemispheres and vermis) and the hippocampus (hypoplasia or
163 malrotation) are components of a larger spectrum of structural abnormalities including extra-
164 axial CSF fluid increases, corpus callosum abnormalities, choroid plexus abnormalities and
165 brainstem dysplasia that we have recently observed in both human CHD patients and preclinical
166 CHD mouse models.^{10,30-35} As such, we have derived a composite Brain Dysplasia Score (BDS)
167 which was previously created with one point given for each positive finding in any of thirteen
168 parameters including: hypoplasia in cerebellar hemispheres and vermis; dysplasia in cerebellar
169 hemispheres and vermis; supratentorial extra-axial fluid; dysmorphometry of left and right
170 olfactory bulbs and sulci; abnormalities in hippocampus and choroid plexus; malformation of
171 corpus callosum; and brainstem dysplasia.^{10,30-35} There is little known about the relationship of
172 these milder structural dysplastic abnormalities (relative to more gross brain malformation) to
173 white matter connectivity.

174 Here, we sought to use our quantitative data-driven approach to primarily correlate
175 clinical risk factors in CHD neonates to abnormalities of white matter connectivity using two
176 complementary techniques: structural network topology (connectome) and seed based
177 tractography. We first compared patient specific and preoperative clinical factors to network
178 topology and tractography alterations on a preoperative neonatal brain MRI, and intra and
179 postoperative clinical factors to network topology alterations on postoperative neonatal brain
180 MRI. Secondly, we correlated our previously derived total BDS score (and its subcortical
181 components including olfactory, cerebellar, and hippocampal dysmaturation) with similar
182 methodologies as our primary aim including structural network topology (connectome) and seed-
183 based tractography measurements. As such, we tested the hypothesis that clinical risk factors
184 would predict distinct patterns of microstructural brain dysmaturation compared to those patterns
185 predicted by the total BDS score/subcortical components.

186 187 **METHODS**

188 Patients with critical CHD were recruited both pre- and postnatally for consecutive
189 enrollment in this prospective, observational neuroimaging study at two large children's
190 hospitals (Children's Hospital Los Angeles and Children's Hospital of Pittsburgh). Critical CHD
191 was defined as defects expected to require corrective or palliative cardiac surgery within the first
192 month of life. Patients that had a known major chromosomal abnormality, were premature (≤ 36
193 weeks of age), died prior to MRI or had no MRI performed, or did not require neonatal cardiac
194 surgery were excluded. The data collection sources included the electronic medical record.
195 Clinical data collection included 18 patient-specific and 9 preoperative variables associated with
196 preoperative scan and 6 intra-operative (e.g. cardiopulmonary bypass, deep hypothermic
197 circulatory arrest times) and 12 postoperative variables associated with postoperative scan that
198 were selected based on prior literature on neurodevelopmental research in CHD as well as
199 criteria included in the RACHS-1 scoring system. These are listed in **Table 1**.^{14,36-38} CHD
200 lesions were classified in several ways (not mutually exclusive) including cyanotic vs. acyanotic
201 defects, presence of aortic arch obstruction, single vs. double ventricle defects, presence of d-

202 TGA, presence of a conotruncal defect (which includes d-TGA as well as other lesions with
203 altered conal septal/outflow tract relationships such as tetralogy of Fallot, double outlet right
204 ventricle, truncus arteriosus, etc.), and presence of heterotaxy. CHD lesions were additionally
205 classified by impairment of fetal substrate delivery, i.e. how a CHD lesion impacts the fetal
206 circulation which aims to direct the highest oxygen and nutrient rich blood from the placenta
207 toward the fetal brain. This severity score included normal (isolated septal and arch defects),
208 altered (which includes single ventricles, tetralogy of Fallot, and other lesions which have fetal
209 intracardiac mixing), and severely altered (which includes d-TGA and its variants which results
210 in direction of the least oxygen and nutrient rich blood to the fetal brain)¹³. Parental consent was
211 obtained, and the institutional review boards of both institutions approved the study.

212
213 **Neonatal Brain MRI Protocol:** Preoperative brain imaging was conducted when the
214 cardiothoracic intensive care unit (CTICU)/cardiology team determined the patient was stable for
215 transport to the MRI scanner. A postoperative scan was performed when the patient was younger
216 than 3 months of postnatal age either as an inpatient or outpatient. Most of our scans were
217 research indicated and, as such, no additional sedation/anesthesia was given for purpose of the
218 scan. Most of the preoperative scans were performed on non-intubated, non-sedated patients;
219 however, if a patient was intubated and sedated for clinical reasons at the time of the scan, their
220 clinically indicated sedation continued under care of the primary CTICU team. The postoperative
221 scans were performed after the infant had stepped down from the CTICU and were done as “feed
222 and bundle” scans without sedation.

223
224 MR data were acquired on a Philips 3T Achieva MR System (Ver. 3.2.1.1; Philips Healthcare,
225 Foster City, California) with the use of either a neonatal SENSE coil or a standard 8-channel
226 SENSE head coil. To minimize movement during imaging, infants were secured in Med-Vac
227 Immobilization Bag (CFI Medical, Fenton, Michigan) with multiple levels of ear protection,
228 including ear plugs, MiniMuffs (Natus Medical Inc, Pleasanton, California), and standard
229 headphones. Conventional T1-weighted, T2-weighted, and diffusion-weighted images were
230 acquired and reviewed by 2 pediatric neuroradiologists for evidence of punctate white matter
231 lesion, acute focal infarction, and hemorrhage as described previously.²³

232 233 MR Acquisition

234 At both sites, a 3T scanner was used for all studies; scans were acquired on a Phillips Achieva at
235 CHLA and Siemens Skyra or GE Excite at CHP. Newborns were positioned in the coil to
236 minimize head tilting. Newborns were fitted with earplugs (Quiet Earplugs; Sperian Hearing
237 Protection, San Diego, CA) and neonatal earmuffs (MiniMuffs; Natus, San Carlos, CA). An
238 MR-compatible, vital signs monitoring system (Veris, MEDRAD, Inc. Indianola, PA) was used
239 to monitor neonatal vital signs. All scans were performed using a multi-channel head coil.
240 Volumetric 3D T1 and T2 imaging and a blood sensitive sequence (GRE or SWI) were
241 performed to evaluate for punctate white matter injury and to evaluate for other major forms of
242 brain injury (infarcts and hemorrhage) and congenital brain malformations. 2D EPI-DTI with 42
243 directions, TE/TR= 92 ms/12600 ms, b = 1000 s/mm², 2 mm slice thickness were acquired; in-
244 plane resolution was close to 2 mm but varied slightly for some participants.

245 246 Data analysis

247 Analyses were performed using in-house routines in IDL (ENVI, Boulder, CO); and routines in

248 SPM8 (Wellcome Dept. of Cognitive Neurology, London, UK), FSL (fMRIB, Oxford, UK), and
249 Brain Connectivity Toolbox (BCT; Indiana University, Bloomington, IN). A schematic of the
250 graph analysis pipeline is presented in Figure 1.

251

252 Pre-processing and Generation of FA-independent Developing White Matter Segmentation

253 Data that was automatically upsampled (factor = 2) by the scanner reconstruction software (in
254 GE scanners) was corrected by rebinning the data in the in-plane directions by a factor of 2.
255 Frames with slice drop-out artifacts were removed using an automated routine in IDL. Motion
256 and eddy current artifacts were corrected using routines in FSL, and maps of FA, axial
257 diffusivity, radial diffusivity, and direction of principal eigenvector computed. The B_0 maps
258 were normalized to the neonatal anatomical template³⁹ using routines in SPM8 and these
259 transformations were used to applied to the FA maps (resampled to 2 mm isotropic resolution).
260 An average study specific FA template was then constructed in template space. The FA template
261 was back-transformed into native space for each participant (using routines in SPM8 and the
262 individual FA map as the reference) and the neonatal cortical parcellation atlas³⁹ was also
263 transformed into native space using that transformation.

264 In the population studied, FA maps cannot be directly used in deterministic tractography due to
265 within participant variations in FA values associated with post-conceptual age, CHD status,
266 regional differences in myelination status, and other factors. To account for FA variations, WM
267 probabilistic maps were computed from segmentations performed using the FA map, the
268 neonatal WM, gray matter, and CSF templates³⁹ using `spm_preproc8` routine in SPM8. These
269 WM probability map computed are not dependent on the absolute values of FA in white matter
270 and were used for the deterministic tractography.

271

272 Tractography and Construction of Unweighted and Weighted Graph Matrices

273 Deterministic tractography in native space was carried out using routines in IDL. Streamlines
274 were constructed starting from each voxel with WM probability > 0.78 and were continued in
275 both directions with stopping criteria of turning angle > 45 degrees or WM probability < 0.78
276 (using the white matter template). This threshold was determined via visual inspection to
277 optimize the tradeoff between ensuring all streamlines remain in white matter and ensuring
278 streamlines do not end prematurely due to a misclassified voxel. Secondary analyses showed
279 that variation of this parameter did not appreciably affect cost and global efficiency (details in
280 Appendix). Using the parcellation atlas (transformed into native space) to identify the cortical
281 regions at both ends of each streamline we generated three 90 x 90 matrices using two different
282 weighted matrices and one unweighted matrix). One of the two weighted approaches was termed
283 “average FA” (each non-diagonal element contains the FA averaged over all streamlines
284 connecting two regions, and the other weighted approach was termed “number of tracts” (each
285 non-diagonal element contains the total number of streamlines connecting the two regions). The
286 unweighted approach was termed “adjacency” (each non-diagonal element is either 0 or 1,
287 depending on whether at least one tract connects the corresponding cortical regions). See **Figure**
288 **2** for a schematic of these 3 weighted methods. We interpreted these difference in weighting as
289 follows: “microstructural” changes reflect more in mean FA weighting while “macrostructural”
290 change reflects more the other weighted approach “number of tracts” and the unweighted
291 approach “adjacency”. Of note, the “number of tracts” approach likely also weights towards
292 total white matter volume.

293

294 Graph Analysis

295 Unweighted (for adjacency matrices) and weighted (for number of tracts and average FA
296 matrices) metrics were computed using routines in the C++ version of BCT and in-house
297 routines in IDL. Global metrics computed included cost (number of connections), global
298 efficiency, transitivity, modularity, and small-worldness. Nodal metrics (which have a value for
299 each of the 90 nodes) (see **Supplemental Table 1** for anatomic labels) computed included
300 clustering coefficient, nodal efficiency, eigenvector centrality, and participation coefficient
301 (adjacency matrices only). As the modularity and small-world calculations depend on a
302 stepwise optimization from a random starting point, 100 iterations were used, and the results
303 were averaged (small-world) or maximum value was used (modularity). Additionally, we
304 examined our nodal level results in context of the developing brain network topology in the last
305 trimester and early infancy⁴⁰⁻⁴⁶.

306

307 **Graph Analysis:**

308 Graph metrics (global efficiency, modularity, transitivity and small-worldness) were computed
309 via the C++ modules available from the Brain Connectivity Toolbox (BCT; Indiana University).
310 A brief description for each metric is given below^{16,47}. *Global efficiency* is a measure of network
311 integration^{16,48}. The *path length* between two nodes is defined as the shortest distance between
312 them. Global efficiency is defined as the mean of the reciprocal path length over all pairs of
313 nodes (e.g. if every node was directly connected to every other node, the path lengths would all
314 be one, and global efficiency (mean(1/path length) would be 1). In a highly integrated network,
315 the typical number of steps it takes to get from one node to another is low. *Modularity* is a
316 measure of network segregation^{49,50}. Modularity is defined as the fraction of the edges that fall
317 within given modules minus the expected such fraction if the edges were distributed at random.
318 In a more modular – or segregated – network, nodes within a given module are more highly
319 interconnected, and less connected to nodes outside the module. Modularity was calculated using
320 the Louvain algorithm⁵¹. *Transitivity*, another measure of segregation at the local or nodal level,
321 is calculated as the proportion of triangles (i.e., where A–B, A–C and B–C are all directly
322 connected) relative to incomplete triangles (i.e., where A–B and A–C are directly connected, but
323 B–C are not) and quantifies the frequency of localized clusters within the overall network.
324 *Small-worldness* represents the balance of integration and segregation^{52,53}. Small-worldness is
325 calculated as the ratio of transitivity to characteristic path length, divided by the ratio of
326 transitivity to characteristic path length for a random graph with the same degree distribution;
327 and quantifies the extent to which the network balances overall efficiency and localized
328 clustering⁵⁴. In a small-world network, there is only a slight increase in characteristic path length
329 as compared to a random network (and hence only slightly less integration), but a large increase
330 in transitivity (and hence much greater segregation).

331

332 **Brain Dysplasia Score (BDS) Methods:**

333 The BDS was based on previous correlative analysis of brain phenotype from CHD mouse
334 mutant and human infant MRI including a spectrum of subtle brain dysplasia (hypoplasia or
335 aplasia) including increased extra-axial CSF and abnormalities of the olfactory bulbs,
336 cerebellum, hippocampus and corpus callosum and a composite brain dysplasia score, as
337 previously described.^{10,30-35} Basic pediatric neuroradiological definitions and criteria were used
338 from Barkovich et al. for overall assessment of brain abnormalities.⁵⁵ For olfactory
339 abnormalities, we assessed for aplasia/hypoplasia of the olfactory bulb within the olfactory

340 groove and aplasia/hypoplasia of the olfactory sulcus on high resolution coronal T2 images.⁵⁶
341 Hippocampal abnormalities (hypoplasia/malrotation/inversion) were identified as previously
342 described on coronal T1 and T2 images.⁵⁷⁻⁶¹ Brainstem dysplasia including either
343 hyperplasia/hypoplasia and asymmetry/disproportion of the any part of the brainstem (medulla,
344 pons, midbrain) using sagittal and axial T1/T2 imaging based on prior studies by Barkovich et
345 al.⁶² Corpus callosum dysplasia included focal hypogenesis, asymmetry/disproportion of
346 different portions of the corpus callosal (genu, body, splenium, rostrum), or overall abnormal
347 “arching” or morphology best identified on Sagittal T1/T2 imaging as previously described by
348 Barkovich et al.⁶³ A composite was created with one point given for each positive finding in
349 any of thirteen parameters including: hypoplasia in cerebellar hemispheres and vermis; dysplasia
350 in cerebellar hemispheres and vermis; supratentorial extra-axial fluid; dysmorphometry of left
351 and right olfactory bulbs and sulci; abnormalities in hippocampus and choroid plexus;
352 malformation of corpus callosum; and brainstem dysplasia. Brain injury was assessed using the
353 method described by Licht et al.⁹.

354

355 **Seed-based Tractography Analysis:**

356 **Iterative Mask Set Refinement**

357 To measure the accuracy of our iteratively developed semi-automated method, we first generated
358 a “gold-standard” set by manually delineating the mask sets for the following tracts: genu, body,
359 and splenium of the corpus callosum; anterior and posterior segments of the superior longitudinal
360 fasciculus (SLFA and SLFP, respectively); inferior longitudinal fasciculus (ILF), fronto-occipital
361 fasciculus (FOF), and cortical spinal tract (CST). Manual mask set delineation was performed
362 following the guidelines published by Schneider⁶⁴ et al. The ROIs and ROAs comprising each
363 mask set, and visualization of each manual mask set has recently been published⁶⁵. All subjects
364 from the CHP and CHLA cohorts were manually delineated.

365 The automated tractography was performed by propagating the above mask sets from a cohort-
366 specific template onto each subject’s native space diffusion images. We generated cohort-
367 specific templates using a modified version of the FSL TBSS pipeline⁶⁶. First, we non-linearly
368 co-registering all subject FA maps into a standard space, selecting the most representative
369 subject and setting it as the new standard space for subsequent registrations. All subjects were
370 then non-linearly transformed into this new space, generating a new cohort-specific atlas. This
371 process is iterated until no measurable improvement in registration is perceived. We then
372 duplicating the above mask sets, following the identical anatomical guidelines, onto each the
373 generated cohort template. The masks were then propagated into each subject’s native diffusion
374 space using the previously calculated non-linear transforms. Each tract was delineated in DSI
375 studio using a deterministic tracking algorithm an FA threshold of 0.1 and angular threshold of
376 45 degrees with no manual pruning. We used four increasingly granular metrics to measure the
377 accuracy of the semi-automated approach. At each successive mask-refinement iteration, more
378 emphasis is placed on the more granular measure. First, as a qualitative measure of cohort-level
379 accuracy, we projected both the manually delineated tracts and automated tracts onto the cohort-
380 specific atlas, displaying the spatial distribution of each tract and level of agreement. This allows
381 for the detection of obvious points of failure in the pipeline, as well as a general overview of the
382 variance in anatomical tract location. Further refinement used DICE coefficients to compare
383 automated vs. manual tractography, and finally, along-tract measures of dispersion within cohort

384 was the final quality check to validate the automated approach. All tractography values used in
385 this hypothesis-driven analysis used the output of the automated pipeline.

386
387 **Statistical Analysis:** Multivariable regression with false discovery rate (FDR) correction was
388 used, with covariates including postmenstrual age at time of scan. The FDR is one way of
389 conceptualizing the rate of type I errors in null hypothesis testing when conducting multiple
390 comparisons. We defined our “exposure” as the patient and clinical factors and the
391 “neuroimaging outcome measure” as cost (number of connections) and global and nodal
392 efficiency (network integration) as the outcome, in each of the 3 differentially weighted
393 connectome methods (average FA, number of tracts, and adjacency connectomes). The patient
394 and clinical risk factors were then additionally compared against seed-based tractography
395 (including FA, radial diffusivity, and axial diffusivity. Patient specific, cardiac lesion subtype,
396 and preoperative variables were compared only with the preoperative MRI scans. The
397 intraoperative and postoperative exposures were compared only with the postoperative MRI
398 scans. The BDS, its individual components of cerebellar, olfactory and hippocampal
399 abnormalities, as well as presence of brain injury (punctate WMI and stroke) were evaluated
400 against the 3 connectome methods on both pre and postoperative MRI timepoints. The BDS and
401 its individual components of cerebellar, olfactory, and hippocampal abnormalities were
402 evaluated against tractography by FA, radial and axial diffusivity at preoperative and
403 postoperative time points as well as on all scans combined.

404
405 **Outcomes:** The primary neuroimaging outcomes for the study were cost and global and nodal
406 efficiency (connectome) and fractional anisotropy (seed-based tractography). The secondary
407 outcomes were (connectome) modularity and small-worldness (connectome) and radial and axial
408 diffusivity (seed-based tractography).

409 410 **RESULTS**

411 Two hundred ninety-one subjects were enrolled from June 2009 to October 2016. Of
412 these subjects, 158 met exclusion criteria including 57 with no MRI done, 38 due to prematurity,
413 38 passed the age threshold, 11 expired preoperatively, 10 had no neonatal surgery and 4 had a
414 postnatal major genetic diagnosis. Of the 133 term CHD infants with brain MRI meeting
415 inclusion criteria, 110 subjects had sufficient imaging quality for DTI analysis and comprised the
416 study group, including 57 from Children’s Hospital Los Angeles and 53 from Children’s
417 Hospital of Pittsburgh. This group included 67 preoperative MRI scans and 77 postoperative
418 MRI scans (**Figure 3**).

419 **Table 1** lists patient demographic data and clinical factors. The majority of the CHD
420 neonates were male (73%), had cyanotic forms of CHD (90%) including 48% with single
421 ventricle CHD and 35% with d-TGA, and had surgery involving cardiopulmonary bypass (88%),
422 with an average cardiopulmonary bypass time of 86 ± 56 minutes. Postoperatively, 20% were on
423 extracorporeal membrane oxygenation (ECMO), 14% had seizures, and 9% required
424 cardiopulmonary resuscitation during the first hospitalization. The mortality rate for the study
425 population prior to discharge was 6%.

426 **Clinical Risk Factors vs Connectome**

427 ***Patient and Prenatal Factors-Correlation with Connectome Measures (Table*** 428 ***2(A),2(B),2(C)):***

429 We analyzed the patient-specific and CHD subtype factors against the 3 differentially
430 weighted connectome analyses on preoperative scans and found several CHD subtypes were
431 related to alterations in global network topology (**Table 2(A-C)**). Aortic arch obstruction (in
432 both single and 2-ventricle patients combined) predicted altered modularity by all 3 connectome
433 methods ($p = -0.0106$ for adjacency, -0.0098 for number of tracts, and -0.0183 for average FA
434 connectome), as well as small-worldness in the number of tracts ($p = -0.0141$) and average FA ($p =$
435 -0.0039) connectomes. D-TGA predicted altered modularity ($p = 0.0009$) and reduced cost ($p =$
436 0.0442) in the adjacency connectome, as well as reduced cost ($p = -0.0043$), global efficiency ($p =$
437 0.0058) and transitivity ($p = -0.0203$) in the number of tracts connectome, and increased
438 modularity ($p = 0.0237$) and small-worldness ($p = 0.0353$) in the average FA connectome. The
439 prenatal cerebral substrate delivery severity score, which separated CHD lesions by how much
440 alteration there is in the typical fetal circulation which directs the highest oxygen and nutrient
441 rich blood from the placenta to the fetal brain, was also a strong predictor of lower cost ($p =$
442 0.0073) and global efficiency ($p = -0.0054$) in the number of tracts connectome. Conotruncal
443 CHD subtype (which includes d-TGA as well as other lesions with altered conal septal/outflow
444 tract relationships such as tetralogy of Fallot, double outlet right ventricle, truncus arteriosus, etc)
445 predicted modularity ($p = 0.0075$) and small-worldness ($p = 0.0305$) in the average FA
446 connectome. Assortativity was not associated with the CHD subtypes by any of the methods.
447 The only biometric parameter found to have an association was head circumference percentile
448 which had a weak relationship with reduced global efficiency ($p = -0.0439$) and the only
449 preoperative variable with a network topology association was preoperative arterial blood gas pH
450 predicting reduced cost ($p = -0.0444$). These results are given in **Table 2(A-C)**.

451 In the analysis of nodal network topology, increased severity of fetal cerebral substrate
452 delivery was associated with reduced nodal efficiency in multiple areas, shown in **Figure 4**,
453 (anatomic location of nodes – Precuneus Right (PCUN-R), Postcentral Gyrus Right (PoCG-R),
454 Precentral Gyrus Right (PreCG-R), Supplementary Motor Area Right (SMA-R), Middle Frontal
455 Gyrus Right (MFG-R), Thalamus Right (THA-R), Superior Temporal Gyrus Right (STG-R),
456 Hippocampus Right (HIP-R), Insula Right (INS-R), Caudate Right (CAU-R), Anterior Cingulate
457 Gyrus Right (ACG-R), Superior Frontal Gyrus Medial Right (SFGmed-R).

458 459 ***Intraoperative Factors (Table 2(A),2(B),2(C)):***

460 Associations between intraoperative factors and global network topology on the
461 postoperative MRI were as follows: Time on cardiopulmonary bypass was associated with
462 decreased cost ($p = -0.0271$), global efficiency ($p = -0.0373$) and transitivity ($p = -0.0173$) in the
463 average FA connectome. Use of circulatory arrest/DHCA (deep hypothermic circulatory arrest)
464 was associated with decreased assortativity in all 3 connectome methods ($p = -0.0051$ for
465 adjacency, number of tracts and average FA) and minutes of circulatory arrest/DHCA were
466 associated with alterations of small-worldness in the adjacency ($p = 0.031$) and average FA
467 ($p = 0.0247$) connectomes. (**Table 2(A-C)**). There were no significant associations at a nodal level
468 with the intraoperative factors.

469
470
471

472 **Postoperative Factors (Table 2(A),2(B),2(C)):**

473 In the global network topology analysis (Table 2(A-C)), postoperative seizures were
474 associated with decreased cost in the adjacency connectome ($p=-0.0388$) and with reduced global
475 efficiency in the average FA connectome ($p=-0.0496$). Time on ECMO predicted reduced cost
476 ($p=-0.404$) and global efficiency ($p=-0.0116$) in the average FA connectome. Undergoing
477 cardiopulmonary resuscitation (including chest compressions) and expiration during the first
478 hospitalization both predicted reduced global efficiency in the average FA connectome ($p=-$
479 $0.0318, -0.0361$ respectively).

480 In the nodal analysis by postoperative time points, having seizures postoperatively and time on
481 ECMO both demonstrated multiple associations with decreased efficiency in nodal areas, shown
482 in Figure 4 [anatomic location of nodes- *Seizures Post-Operative MR Scan*: Superior Occipital
483 Gyrus Right (SOG-R), Middle Occipital Gyrus Right (MOG-R), Calcarine Right (CAL-R),
484 Heschl Right (HES-R), Putamen Right (PUT-R) *ECMO Post-Operative MR Scan*: Superior
485 Parietal Gyrus Right (SPG-R), Postcentral Gyrus Right (PoCG-R), Supramarginal Gyrus Right
486 (SMG-R), Middle Central Gyrus Right (MCG-R), Rolandic Operculum Right (ROL-R),
487 Thalamus Right (THA-R), Hippocampus Right (HIP-R), Putamen Right (PUT-R), Pallidum Right
488 (PAL-R), Caudate Right (CAU-R), Superior Frontal Gyrus Medial Right (SFGmed-R)]

489

490 **Clinical Risk Factor vs Tractography**

491 The clinical risk factors were analyzed against tractography including FA, radial
492 diffusivity, and axial diffusivity of the following areas: genu, body, and splenium of the corpus
493 callosum, right and left CST, FOF, ILF, SLF.

494

495 **Clinical Risk Factor vs Fractional Anisotropy (Supplemental Table 2(A-D)):**

496 When the clinical risk factors were compared against DTI tractography by FA, several
497 intraoperative variables were found to have association with postoperative FA tractography
498 outcomes. Time on cardiopulmonary bypass correlated with mean FA of the left FOF
499 ($p=0.0242$). Aortic cross-clamp time was associated with abnormal FA of the genu and splenium
500 of the corpus callosum ($p=0.0033$ for both, Supplemental Table 2 (C)). After FDR correction,
501 tractography by FA did not have significance with any of the patient-specific, CHD subtype,
502 preoperative, or postoperative clinical parameters (Supplemental Table 2(A),(B),(D)).

503

504 **Clinical Risk Factor vs Radial Diffusivity (Supplemental Table 2(A-D)):**

505 When the clinical risk factors were compared against DTI tractography by radial
506 diffusivity, multiple associations were found with the patient-specific factors specifically the
507 neonatal anthropometric parameters and preoperative scans (Supplemental Table 2(A)).
508 Newborn biometry was predictive of increased radial diffusivity of the genu, body, and splenium
509 of the corpus callosum including birth weight ($p=0.041$ genu, 0.0066 body, 0.0176 splenium),
510 birth weight percentile ($p=0.0055$ genu, 0.0022 body, 0.0055 splenium), head circumference ($p=$
511 0.0147 genu & body, 0.0198 splenium), and birth length percentile ($p=0.0407$ for all 3). Birth
512 weight was also predictive of increased radial diffusivity of the left SLF ($p=0.0187$) and birth
513 weight percentile with increased radial diffusivity of the right CST ($p=0.02$), left FOF and right
514 ILF ($p=0.0426$), both right and left SLF ($p=0.0297$ R and 0.02 L). Head circumference
515 percentile predicted increased radial diffusivity of the left FOF ($p=0.0147$), and birth length
516 percentile of the inferior ($p=0.0407$ R and L) and SLF ($p=0.0407$ R, 0.0418 L). The 1-minute

517 APGAR score correlated with increased radial diffusivity of the corpus callosum body, left FOF,
518 left ILF, and right SLF ($p=0.0204$ for all).

519 Among the intra-operative factors, cardiopulmonary bypass time predicted increased
520 radial diffusivity of the left FOF ($p=0.0242$) and aortic cross-clamp time predicted increased
521 radial diffusivity of the genu and splenium of the corpus callosum on postoperative scans
522 ($p=0.0033$) (**Supplemental Table 2(C)**). None of the CHD subtype categories, preoperative
523 clinical factors, or postoperative clinical factors predicted radial diffusivity of any of the
524 structures assessed (**Supplemental Table 2(A),(B),(D)**).

525

526 **Clinical Risk Factor vs Axial Diffusivity (Supplemental Table 2(A-D)):**

527 When the clinical risk factors were compared against DTI tractography by axial
528 diffusivity, the findings were quite similar to those for radial diffusivity. For axial diffusivity,
529 again multiple associations were found with the patient-specific factors specifically the neonatal
530 anthropometric parameters on preoperative scans (**Supplemental Table 2(A)**). Birth weight was
531 predictive of increased axial diffusivity of the corpus callosum body and left SLF ($p=0.0182$).
532 Birth weight percentile predicted increased axial diffusivity of the corpus callosum ($p=0.0072$
533 genu, 0.0066 body, 0.0176 splenium), right CST ($p=0.0114$), left FOF ($p=0.0327$), and both SLF
534 ($p=0.0207$ R and 0.0157 L). Head circumference percentile predicted increased axial diffusivity
535 of the of the corpus callosum ($p=0.0017$ genu, 0.0077 body, 0.0132 splenium) and the left FOF
536 ($p=0.0017$), left ILF ($p=0.0132$), and bilateral SLF ($p=0.0478$ R, 0.0257 L). Birth length
537 percentile predicted increased axial diffusivity of the corpus callosum body ($p=0.0226$) and
538 splenium ($p=0.0315$), right CST ($p=0.0315$), and bilateral ILF ($p=0.0315$ R, 0.0187 L) and SLF
539 ($p=0.0352$ R, 0.0330 L). The 1-minute APGAR score correlated with increased radial diffusivity
540 of the left FOF ($p=0.0231$).

541 Among the intra-operative factors, cardiopulmonary bypass time predicted increased
542 postoperative axial diffusivity of the left FOF ($p=0.0242$) and aortic cross-clamp time predicted
543 increased axial diffusivity of the genu and splenium of the corpus callosum ($p=0.0033$)
544 (**Supplemental Table 2(C)**). None of the CHD subtype categories, preoperative clinical factors,
545 or postoperative clinical factors predicted radial diffusivity of any of the structures assessed
546 (**Supplemental Table 2(A),(B),(D)**).

547

548 **Brain Injury and Brain Dysplasia Score (Including Subcortical Components) Findings**

549 A total of 24 subjects had brain injury (22%) including 12 (11%) with punctate white
550 matter injury, and 6 (5%) with stroke. The majority of the injury was seen on the preoperative
551 scan (83% of punctate white matter injury and 67% of stroke occurred on preoperative scan).
552 Brain dysplasia score was 3.6 ± 3.3 . Brain dysplasia included 21 (19%) with cerebellar
553 hypoplasia/dysplasia, 49 (45%) with olfactory bulb/sulcus abnormality, 45 (41%) with
554 hippocampal hypoplasia/dysplasia.

555

556 **Brain Dysplasia Score (including Subcortical Components) vs Connectome (Table 3)**

557 Brain dysplasia was evaluated against global network topology via the 3 differentially
558 weighted connectome analysis methods at both pre and postoperative time points. BDS was not
559 predictive of brain network topology by any of the methods. However, abnormalities of the
560 cerebellum on preoperative scans predicted reduced cost in all 3 connectomes ($p=-0.0417$
561 adjacency, $p=-0.0117$ number of tracts, $p=-0.0388$ average FA) and reduced global efficiency in
562 the number of tracts connectome ($p=-0.0467$). Abnormalities of the hippocampus on

563 preoperative scans predicted reduced global efficiency ($p = -0.0126$) in the adjacency
564 connectome. Olfactory abnormalities on the preoperative scan predicted increased modularity by
565 the number of tracts connectome ($p = 0.021$).

566 Among the brain injury variables, punctate white matter injury on the preoperative scan
567 predicted reduced cost in the adjacency connectome ($p = -0.0401$), and stroke on the
568 postoperative scan predicted multiple abnormalities in the adjacency connectome including
569 reduced cost ($p = -0.0437$), global efficiency ($p = -0.0285$), transitivity ($p = -0.0439$) and increased
570 modularity ($p = 0.0381$). The composite brain injury did not predict any connectome metrics
571 (**Table 3**).

572 Abnormalities of the subcortical structures including hypoplasia/dysplasia of the
573 cerebellum, hippocampus, and olfactory bulb/sulci predicted altered nodal efficiency in multiple
574 areas ($p < 0.05$, **Figure 5**). The patterns of nodal prediction were unique for each subcortical
575 structures with the hippocampus abnormalities predicting widespread reduced nodal efficiency in
576 all lobes of the brain, the cerebellum abnormalities predicting increased prefrontal nodal
577 efficiency and the olfactory bulb abnormalities predicting posterior parietal-occipital nodal
578 efficiency. The anatomic location of these nodes were : (1) Hippocampal Hypoplasia/Dysplasia:
579 Inferior Temporal Gyrus Left (ITG-L), Amygdala Left (AMYG-L), Putamen Left (PUT-L),
580 Insula Left (INS-L), Caudate Left (CAU-L), Inferior Frontal Gyrus Pars Triangularis Left
581 (IFGtriang-L), Pallidum Left (PAL-L), Superior Frontal Gyrus Medial Left (SFGmed-L),
582 Middle Frontal Gyrus Left (MFG-L), Superior Frontal Gyrus Left (SFGdor-L), Supplementary
583 Motor Area Left (SMA-L), Precentral Gyrus Left (PreCG-L), Paracental Lobule Left (PCL-L),
584 Postcentral Gyrus Left (PoCG-L), Superior Parietal Gyrus Left (SPG-L), Precuneus Left
585 (PCUN-L), Cuneus Left (CUN-L), Calcarine Left (CAL-L), Thalamus Left (THA-L),
586 Hippocampus Left (HIP-L); (2) Cerebellar Hypoplasia/Dysplasia: Gyrus Rectus Left (REC-L),
587 Inferior Frontal Gyrus Pars Triangularis Left (IFGtriang-L), Superior Frontal Gyrus Medial Left
588 (SFGmed-L), Middle Frontal Gyrus Left (MFG-L), Superior Frontal Gyrus Left (SFGdor-L),
589 Precentral Gyrus Left (PreCG-L), Postcentral Gyrus Left (PoCG-L); (3) Olfactory
590 Hypoplasia/Dysplasia: Superior Temporal Pole Left (TPOsup-L), Hippocampus Left (HIP-L),
591 Middle Occipital Gyrus Left (MOG-L), Superior Occipital Gyrus Left (SOG-L), Superior
592 Parietal Gyrus Left (SPG-L), Middle Central Gyrus Left (MCG-L)

593 **Brain Dysplasia Score (including Subcortical Components) vs Tractography (Table 4):**

594 The brain dysplasia metrics were analyzed against tractography including FA, radial
595 diffusivity, and axial diffusivity of the following areas: genu, body, and splenium of the corpus
596 callosum, right and left CST, FOF, ILF, SLF. This analysis took place on preoperative scans,
597 postoperative scans, and all scans combined (**Table 4**).

598 FA of the right CST on all scans combined correlated with global brain dysplasia score
599 (BDS) ($p=0.0495$) and FA of the bilateral CST correlated with cerebellar dysplasia ($p=0.0036$ R,
600 $p=0.0223$ L) for all scans combined as well as for the preoperative scans only ($p=0.0288$ R).

601 Radial diffusivity of multiple tracts demonstrated multiple correlations with brain
602 dysplasia parameters. Radial diffusivity of the corpus callosum correlated with BDS on
603 preoperative scans alone ($p=0.0029$ genu, 0.0173 body, 0.002 splenium) and all scans combined
604 ($p=0.025$ genu, 0.0086 splenium), with cerebellar hypoplasia/dysplasia on preoperative only
605 scans ($p=0.0275$ genu, 0.0391 body, <0.0001 splenium) and all scans combined ($p=0.0004$
606 splenium), and hippocampal hypoplasia/dysplasia on both preoperative only scans ($p=0.0133$
607 genu, 0.0002 body, 0.0004 splenium) and all scans combined ($p=0.0282$ genu, 0.0029 body,
608 0.0005 splenium). Radial diffusivity of the left FOF correlated with BDS ($p=0.0415$) and
609 hippocampal abnormalities ($p=0.0034$) and of the right FOF with cerebellar anomalies
610 ($p=0.0459$) all on preoperative scans. Radial diffusivity of the left ILF correlated with BDS on
611 preoperative ($p=0.018$) and all scans ($p=0.0044$), with cerebellar abnormalities on preoperative
612 ($p=0.0287$) and all scans ($p=0.0088$), and with hippocampal abnormalities on preoperative
613 ($p=0.0054$) and all scans ($p=0.082$). Radial diffusivity of the right SLF was associated with
614 hippocampal abnormalities on preoperative only scans ($p=0.0449$).

615 Axial diffusivity of multiple tracts also demonstrated correlations with brain dysplasia
616 parameters. Axial diffusivity of the corpus callosum correlated with BDS on preoperative scans
617 alone ($p=0.0194$ genu, 0.0371 body, 0.0029 splenium) and all scans combined ($p=0.0262$
618 splenium), with cerebellar abnormality on preoperative only scans ($p=0.0251$ genu, <0.0001
619 splenium) and all scans combined ($p=0.0004$ splenium), and hippocampal abnormality on both
620 preoperative only scans ($p=0.0212$ genu, 0.0005 body, 0.0003 splenium) and all scans combined
621 ($p=0.0007$ splenium). Axial diffusivity of the left CST was associated with hippocampal
622 abnormality on all scans combined ($p=0.0428$). Axial diffusivity of the left FOF correlated with
623 hippocampal abnormalities ($p=0.006$) and of the right FOF with cerebellar anomalies ($p=0.0495$)
624 on preoperative scans. Axial diffusivity of the left ILF correlated with BDS on preoperative
625 ($p=0.0464$) and all scans ($p=0.0127$), with cerebellar abnormalities on preoperative ($p=0.0422$)
626 and all scans ($p=0.007$), and with hippocampal abnormalities on preoperative ($p=0.0082$) and all
627 scans ($p=0.0109$). Axial diffusivity of the right SLF was associated with hippocampal
628 abnormalities on preoperative scans ($=0.0263$).

629 DISCUSSION

630 Neurodevelopmental deficits are common in infants with congenital heart disease (CHD)
631 who undergo neonatal open-heart surgery.^{4,67-69} Some risk factors for these deficits are innate
632 (e.g. genetic), but others involve modifiable medical management.^{26,70-74} The pathophysiology
633 of CHD -related neuropsychological impairment is multifactorial, likely acting through two
634 broad mechanistic pathways, destructive and developmental.⁷⁵ This *destructive-developmental*
635 *amalgam* is mediated by exposure to potentially toxic agents (e.g. volatile anesthetic agents,
636 inflammation) or deprivation of essential exposures (e.g. oxygen).⁷⁵ This amalgam includes
637 diffuse white matter injury (WMI), cortical long-range connectivity, and focal WMI all of which
638 is likely to impact diffusion tensor imaging measures, either post-processed by connectome or
639 tractography techniques. Overall, this is the first study to use the brain connectome to look at the
640 interaction of clinical factors and novel properties of brain tractography, specifically cost, global
641 efficiency and modularity.

642 One of our major findings was that d-TGA anatomy and a 3-tiered severity score based
643 on alteration of fetal substrate delivery were both found to be associated with white matter
644 network topology including lower cost and reduced global efficiency when looked at through a
645 number of tracts connectome analysis, which is weighted toward brain volume. We found that d-
646 TGA additionally resulted in lower cost, revealed from a macrostructure perspective in our
647 adjacency analysis. The altered fetal substrate delivery severity score also had multiple nodal-
648 level connectome alterations (**Figure 4**). Interestingly, the fact that d-TGA patients tend to have
649 the most impaired prenatal cerebral oxygen and substrate delivery¹³ may be a driving factor for
650 these perturbations given that patients with d-TGA rarely have identifiable chromosomal or
651 genetic abnormalities, making genetic underpinnings seem less likely. Remarkably, a previous
652 connectome study also showed that adolescents with d-TGA had reduced global efficiency and,
653 importantly, these network properties mediated poor neurocognitive outcomes in d-TGA patients
654 compared to their referent adolescents across every domain assessed⁷⁶. This has important
655 implications to suggest that neurocognitive perturbation is mediated by global differences in
656 white matter network topology, which are already present in the preoperative neonatal time
657 period.

658 Our secondary connectome outcome measures included brain network modularity and
659 small-worldness. Conotruncal cardiac defect subtype (which includes d-TGA but also several
660 other cardiac lesions) predicted increased modularity by all 3 weighted methods, and predicted
661 increased small-worldness by the number of tracts and average FA methods (based on volume
662 and microstructure). D-TGA alone, but not altered fetal cerebral substrate delivery, predicted
663 increased modularity and small-worldness in the microstructure/fiber density-weighted model
664 only. Interestingly, a previous study in adolescents with d-TGA also showed both increased
665 modularity and small-worldness, suggesting that both our primary and secondary outcome
666 network abnormalities seen in neonates have potential to persist over the lifetime⁷⁶. Despite their
667 low postoperative morbidity and the rarity of need for reinterventions after an initial arterial
668 switch operation, d-TGA patients have been shown to have suboptimal neurodevelopmental
669 outcomes extending into adolescence as shown by the Boston Circulatory Arrest Study
670 (BCAS).^{4,67-69}

671 In contrast to increased modularity seen in conotruncal and d-TGA subjects, aortic arch
672 obstruction was found to be associated with decreased modularity and decreased small-
673 worldness by all 3 weighted connectome methods. Our study's arch obstruction group consisted
674 largely of single ventricle subjects with arch obstruction (87% of that group), i.e., infants with

675 hypoplastic left heart syndrome and its variants, a group with a large burden of
676 neurodevelopmental disability⁷⁷⁻⁷⁹. Others have implicated problems with modularity with
677 childhood-onset schizophrenia (Alexander-Bloch 2010) and autism (Shi 2013), but this has yet to
678 be studied in neonates with CHD. Further work is needed to understand specifically why
679 modularity is decreased in patients that had arch obstruction and what implications that has on
680 their neurodevelopment.

681 Our connectome results are in contrast to another study evaluating global network
682 organization in neonates with CHD prior to heart surgery⁸⁰. Asis-Cruz et al found similar global
683 efficiency, cost and small world levels in CHD infants compared to healthy controls, and
684 concluded that the brain's ability to transfer information efficiently is maintained in CHD. Of
685 note, this differs from our present study because it was a grouped analysis of 30 CHD subjects of
686 which 7 had d-TGA, whereas our significant findings involving cost and global efficiency were
687 in a subset of infants with d-TGA; additionally they utilized connectome analysis of blood
688 oxygen level dependent imaging while our study utilized DTI. Similar to our present findings,
689 our group's prior work which compared a group of CHD infants to control infants using a similar
690 DTI-based connectome via 3 weighted methods, detected reductions in cost and global efficiency
691 in CHD infants compared to controls, as well as increased small-worldness after controlling for
692 cost, in a population which overlaps the group of our present study and included about 25% d-
693 TGA in the CHD subjects, compared to 35% in our present study.

694 Our second major finding was that certain intraoperative and post-operative risk factors
695 correlated with decreased cost and global efficiency in the average FA matrix postoperatively.
696 This is the connectome method weighted to microstructure and fiber density, and we found that
697 both longer time on cardiopulmonary bypass intraoperatively and longer time on ECMO
698 postoperatively were associated with reduced numbers of connections and reduced network
699 global efficiency. While we know that patients with congenital heart disease that survive ECMO
700 have worse neurodevelopmental outcomes⁴, little is known about early markers of differences in
701 brain connectivity in relation to life-support needs. In fact, one group looked at infants that were
702 placed on ECMO compared to healthy full term controls and found that the ECMO patients
703 (albeit not with CHD) had significant differences in FA measured on DTI in multiple regions⁸¹.
704 Similarly we found significant differences in our ECMO patients when using FA, specifically
705 decreased number of connections and brain integration (global efficiency). Recently in a porcine
706 model, Stinnett⁸² et al looked at cardiopulmonary bypass-induced FA alterations after heart
707 surgery and found, similar to our findings, decreased FA⁸². Specifically they found the most
708 alterations in the frontal cortex and suggested that that may be an early biomarker for white
709 matter injury after cardiopulmonary bypass. An additional postoperative association in our data
710 was with postoperative seizures and lower cost seen in both the average FA and adjacency
711 connectome models. This suggests that seizures are associated with reduced number of
712 connections on both macrostructure and microstructure levels. It is interesting that these the 2
713 clinical factors of time on ECMO and presence of seizures showed similar alterations in brain
714 cost, as in our previous study we found these same clinical factors to both be related to altered
715 brain metabolism (reduced white matter N-acetyl aspartate postoperatively) in a similar way⁸³.
716 Finally, our present study found that reduction in global efficiency on a microstructural level
717 correlated with infants who received cardiopulmonary resuscitation (including chest
718 compressions) and in infants who did not ultimately survive to hospital discharge.

719 The preclinical justification for also using tractography measurements was demonstrated
720 by Morton *et al.* who recently showed that hypoxic exposure of the gyrencephalic piglet brain

721 reduced proliferation and neurogenesis in the postnatal subventricular zone. This resulted in
722 microstructural diffuse WMI as assessed by FA quantitative DTI of long range connectivity of
723 the SLF the FOF, and the ILF the metrics used to calculate the diffuse WMI⁸⁴. This preclinical
724 piglet model also showed reduced cortical maturation similar to human CHD infants, supporting
725 the concept that diffuse WMI also correlates with cortical long-range connectivity-related
726 dysmaturation. Clinically, these DTI findings correlate with neonatal perioperative factors and
727 long-term neurocognitive outcomes in the adolescent BCAS TGA study.^{16,85} Unlike the preterm
728 literature, there are few long-term outcome studies of diffuse WMI in CHD. Beca et al. found
729 relative brain immaturity at 3 months of age was associated with reduced performance in
730 cognition at 2 years of age¹⁴. Serial total brain volumes of d-TGA infants were recently shown to
731 be predictive of 18-month outcomes.⁸⁶ Focal WMI is defined as punctate hyperintensity punctate
732 periventricular fronto-parietal white matter lesions on 3D-T1 peri-operative imaging or “focal
733 non-cystic coagulative necrosis,” involving long-range connectivity crossing-fibers,^{14,24-29} in full-
734 term CHD neonates. Focal WMI has been shown to be predictive of short-term motor
735 impairment in CHD.^{14,24-29}

736 When the clinical risk factors were assessed against conventional DTI tractography,
737 microstructural dysmaturation correlated strongly with birth weight and percentile of weight,
738 length, and head circumference across multiple white matter tracts, suggesting that even among
739 term CHD neonates there is range of brain maturation which varies with the child’s biometry and
740 physical maturation. Reduced FA, and radial and axial diffusivity of the left FOF was correlated
741 with cardiopulmonary bypass time, in line with piglet models of cardiopulmonary bypass using
742 similar techniques⁸², and reductions of all 3 DTI metrics in the corpus callosum with aortic cross-
743 clamp time.

744 It was not surprising that when brain injury was utilized as an exposure for the
745 connectome metrics, punctate white matter injury on preoperative scan predicted reduced cost
746 and stroke on postoperative scan predicted reduced cost and global efficiency; however, these
747 alterations were only seen on a macrostructural level, in the adjacency matrix, and no
748 connectome alterations were seen by the other weighted methods. Of note, the previously
749 discussed connectome analysis excluded patients with injury, so grossly visible injury was not
750 the underpinning of our connectome results discussed above.

751 Subcortical brain dysplasia associations with connectome alterations included 1)
752 cerebellar dysplasia associating with reduced cost by all three weighted methods, 2) reduced
753 global efficiency in the volume-based number of tracts analysis, and 3) hippocampal dysplasia
754 predicting reduced global efficiency on a macrostructural level, in the adjacency connectome.
755 Additionally, hippocampal, cerebellar, and olfactory dysplasia predicted multiple regional
756 patterns of inefficiency on a nodal level, suggestive of regional brain reorganization. Taken
757 together with the associations seen between subcortical dysplasia and tractography analyses,
758 including abnormalities of the hippocampus, cerebellum, and overall BDS predicting widespread
759 microstructural dysmaturation in all white matter tracts evaluated, shared genetic underpinnings
760 to abnormalities of subcortical structure and white matter microstructure are likely.

761

762 **LIMITATIONS**

763 There were several limitations to our study. First, we had a heterogenous group of CHD
764 patients, although they all required neonatal surgery and we subcategorized them into various
765 conceptual categories (single ventricle, arch obstruction, TGA, heterotaxy), a larger sample size
766 of individual defects would help better describe the differences in the brain’s connectome.

767 Additionally, we did not have a healthy control group, rather we compared groups to each other
768 by looking at the clinical variable of interest. We also had normal values for brain network
769 topology from previous studies as well as our previous study comparing CHD to controls that we
770 utilized. In addition, while most of our newborns were not sedated for the MRI, some were
771 sedated for clinical reasons, and we do not know what effect sedation has on brain network
772 topology. Lastly, it will be important to correlate our neuroimaging findings with longer term
773 neurodevelopmental outcomes. How these connectome metrics impact longer-term
774 neurocognition is an important knowledge gap that our study could address with longitudinal
775 follow-up of this enrolled cohort. Future work is needed to also understand how these MR brain
776 studies should become part of clinical practice in the management of these high-risk neonates
777 and be potentially standardized with neurodevelopmental testing.

778

779 **CONCLUSIONS**

780 In summary, our work suggests that microstructural brain connectivity is disrupted in
781 neonates with complex CHD. Prenatal clinical risk factors (heart lesion subtype and prenatal
782 cerebral substrate delivery alterations), major intra and postoperative events (cardiopulmonary
783 bypass time, ECMO time, and seizures) and preclinical CHD-derived subcortical dysplasia were
784 the most predictive of connectome-based neuroimaging outcome measures relative to other pre
785 and postoperative period clinical risk factors, while patient-specific anthropometric
786 measurements (weight, length, and head size percentiles) predicted tractography outcomes. This
787 is in alignment with the evolving literature that most of the neurodevelopmental impairment in
788 CHD is related to patient-specific, prenatal, and unknown genetic factors. Postoperative factors
789 with implications for high neurological severity, including seizures and time on ECMO, were
790 highly predictive of diffuse connective nodal efficiency, identifying high risk patients with poor
791 outcomes. In addition, intraoperative factors (including cardiopulmonary bypass and aortic
792 cross-clamp times) correlated with reduction in tractography metrics, recapitulating
793 microstructural diffusion correlations of white matter injury seen in developmental piglet models
794 of cardiac surgery. Lastly, preclinical-CHD-derived subcortical brain dysplasia scoring
795 predicted more distinct, localized structural network topology patterns in conjunction with
796 tractography-based diffuse microstructural changes, likely reflecting genetic pathways that are
797 known to impact the connectome and alter the organization of white matter development in
798 CHD. Future studies will aim to correlate these findings with long-term neurodevelopmental
799 outcomes in this population.

800

801

802 **FIGURES LEGENDS:**

803 **Figure 1:** Computational pipeline for processing neonatal diffusion tensor imaging data: First a
804 white matter template is generated in MNI space. Second, parcellation is performed using a
805 neonatal AAL template; Third- different weighted matrixes are generated to facilitate network
806 topology measures at the global and the nodal levels.

807

808 **Figure 2:** Theoretical interpretations of the different weighted matrices in relation to cost,
809 micro/macro- organization, fiber density/organization and volume.

810

811 **Figure 3: Study Flow Chart and Recruitment**

812

813 **Figure 4:** Three major clinical risk factors: (prenatal) severity of fetal cerebral substrate delivery
814 correlates with preoperative reduced nodal efficiency in fronto-temporal, paralimbic, and parietal
815 regions; (postoperative) presence of seizures and ECMO predict reduced nodal efficiency in
816 similar regions on the postoperative MRI scan.

817 Severity of Fetal Cerebral Substrate Delivery Pre-Operative MR Scan: Hippocampus Right
818 (HIP-R), Superior Temporal Gyrus Right (STG-R), Thalamus Right (THA-R), Precuneus Right
819 (PCUN-R), Postcentral Gyrus Right (PoCG-R), Precentral Gyrus Right (PreCG-R), Middle
820 Cingulate Gyrus Right (MCG-R), Insula Right (INS-R), Caudate Right (CAU-R), Anterior
821 Cingulate Gyrus Right (ACG-R), Superior Frontal Gyrus Medial Right (SFGmed-R), Middle
822 Frontal Gyrus Right (MFG-R), Supplementary Motor Area Right (SMA-R)

823 Seizures Post-Operative MR Scan: Superior Occipital Gyrus Right (SOG-R), Middle Occipital
824 Gyrus Right (MOG-R), Calcarine Right (CAL-R), Heschl GyrusRight (HES-R), Putamen Right
825 (PUT-R)

826 ECMO Post-Operative MR Scan: Superior Parietal Gyrus Right (SPG-R), Postcentral Gyrus
827 Right (PoCG-R), Supramarginal Gyrus Right (SMG-R), Middle Central Gyrus Right (MCG-R) ,
828 Rolandic Operculum Right (ROL-R), Thalmus Right (THA-R), Hippocampus Right (HIP-R),
829 Putamen Right (PUT-R), Pallidum Right (PAL-R), Caudate Right (CAU-R), Superior Frontal
830 Gyrus Medial Right (SFGmed-R)

831

832 **Figure 5:** A brain dysplasia score (BDS) (composed of hippocampal, cerebellar and olfactory
833 hypoplasia/dysplasia components) predicted specific regional patterns of nodal efficiency
834 suggestive regional brain reorganization and distinct patterns when compared to clinical risk
835 factors demonstrated in Figure 4.

836 Hippocampal Hypoplasia/Dysplasia: Inferior Temporal Gyrus Left (ITG-L), Amygdala Left
837 (AMYG-L), Putamen Left (PUT-L), Insula Left (INS-L), Caudate Left (CAU-L), Inferior
838 Frontal Gyrus Pars Triangularis Left (IFGtriang-L), Pallidum Left (PAL-L), Frontal Superior
839 Gyrus Medial Left (SFGmed-L), Middle Frontal Gyrus Left (MFG-L), Frontal Superior Gyrus
840 Dorsolateral Left (SFGdor-L), Supplementary Motor Area Left (SMA-L), Precentral Gyrus Left
841 (PreCG-L), Paracental Lobule Left (PCL-L), Postcentral Gyrus Left (PoCG-L), Superior Parietal
842 Gyrus Left (SPG-L), Precuneus Left (PCUN-L), Cuneus Left (CUN-L), Calcarine Left (CAL-L),
843 Thalamus Left (THA-L), Hippocampus Left (HIP-L)

844 Cerebellar Hypoplasia/Dysplasia: Gyrus Rectus Left (REC-L), Inferior Frontal Gyrus Pars
845 Triangularis Left (IFGtriang-L), Superior frontal Gyrus Medial Left (SFGmed-L), Middle

846 Frontal Gyrus Left (MFG-L), Superior Frontal Gyrus Left (SFGdor-L), Precentral Gyrus Left
847 (PreCG-L), Postcentral Gyrus Left (PoCG-L)
848 Olfactory Hypoplasia/Dysplasia: Superior Temporal Pole Left (TPOsup-L), Hippocampus Left
849 (HIP-L), Middle Occipital Gyrus Left (MOG-L), Superior Occipital Gyrus Left (SOG-L),
850 Superior Parietal Gyrus Left (SPG-L), Middle Cingulate Gyrus Left (MCG-L)

851 **Table 1. Demographic Characteristics of Final 110 Subjects with Analyzable Diffusion Tensor Imaging (DTI) in Study Group**

	Factor	Total or average (% or SD)
Innate factors and cardiac lesions	Male sex	80 (73%)
	Gestational age at birth, weeks	38.9 (0.9)
	Birth weight, gm and percentile	3,216 (517), 39 (30)
	Head circumference, cm and percentile	34.3 (2.8), 41 (31)
	Birth length, cm and percentile	49.0 (5.9), 36.0 (31.4)
	APGAR at 1 and 5 minutes	7.5 (2), 8.4 (1.2)
	22q11 microdeletion	10 (9%)
	Cyanotic heart disease	99 (90%)
	Arch obstruction	45 (41%)
	Single Ventricle	49 (45%)
	With arch obstruction	39 (35%)
	d-TGA	38 (35%)
	Conotruncal defect	70 (64%)
	Heterotaxy	8 (7%)
	Preoperative factors	Severity of altered fetal cerebral substrate delivery
Normal		11 (10%)
Altered		69 (63%)
Severely altered (d-TGA physiology)		30 (27%)
Preop arterial blood gas pH		7.44 (0.066)
Preop arterial blood gas pO ₂		50.5 (31.8)
Preop arterial lactate (mmol/L)		1.7 (0.7)
Preop renal dysfunction		0
Preop hepatic dysfunction		1 (1%)
Preop inotrope use		44 (40%)
Intraoperative Factors	Age at surgery (days)	6.9 (5)
	Age at surgery ≤ 7 days	81 (67)
	Post-conceptual age at surgery (weeks)	40 (1)
	Cardiopulmonary bypass used	97 (88%)
	Cardiopulmonary bypass time (minutes)	86 (56)
	Aortic cross-clamp used	65 (59%)
	Aortic cross-clamp time (minutes)	41 (39)
	Circulatory arrest/DHCA used	91 (80)
	Circulatory arrest / DHCA time (minutes)	17 (20)
	ECMO during 1 st hospitalization	22 (20%)
Postoperative factors	Time on ECMO (days)	5 (2.5)
	Delayed sternal closure	86 (78%)
	Unplanned intervention(s), 1 st hospitalization (patients)	66 (60%)
	Required CPR, 1 st hospitalization	10 (9%)
	Had seizures during 1 st hospitalization	15 (14%)
	ICU length of stay, 1 st hospitalization (days)	30 (32)
	Hospital length of stay (days)	41 (36)
	Expired during 1 st hospitalization	6 (6%)
Discharged on antiepileptics	12 (11%)	
Discharged with gastrostomy-tube	26 (24%)	
Discharged with tracheostomy and/or ventilator	7 (6%)	

852 d-TGA = d-transposition of the great arteries, CPR = cardiopulmonary resuscitation, DHCA = deep hypothermic circulatory arrest, ECMO =
853 extra corporeal membrane oxygenation, ICU = intensive care unit

854 **Table 2(A). Correlation Between Clinical Risk Factors and Global Connectome Metrics: Adjacency Matrix (FDR-corrected)**

		Cost	Global Efficiency	Transitivity	Modularity	Small World	Assortativity
Innate factors and cardiac lesions	Gestational age at birth	0.3393	0.4742	-0.9632	0.7849	-0.5117	-0.7608
	Birth weight	-0.3771	-0.5902	-0.7142	0.8003	0.8375	-0.9972
	Birth weight percentile	-0.0567	-0.1512	-0.5948	0.2046	0.1767	0.2328
	Head circumference	0.8768	-0.7604	0.9361	-0.9694	0.956	-0.5454
	Head circumference percentile	-0.2892	-0.0439	0.8222	0.3757	0.2501	0.7831
	Birth length	0.8093	0.9694	-0.4568	-0.5394	-0.3504	-0.8874
	Birth length percentile	1	-0.4935	-0.4365	-0.3042	-0.168	0.0565
	APGAR, 1 minute	-0.533	0.5919	-0.2054	-0.4152	-0.8175	-0.334
	APGAR, 5 minute	-0.9119	0.4618	0.4893	-0.833	0.5417	-0.8021
	22q11 microdeletion	-0.5514	-0.2186	-0.6524	0.9916	-0.7051	0.9463
	Single ventricle	0.1528	-0.8881	0.6944	-0.071	-0.232	0.8596
	Arch obstruction	0.572	-0.8024	-0.503	-0.0106	-0.0141	0.2608
	Single ventricle with arch obstruction	0.4095	-0.5173	0.6432	-0.2468	-0.3673	0.1547
	d-TGA	-0.0442	-0.3057	-0.4542	0.0517	0.0849	0.8169
	Conotruncal defect	-0.3726	-0.5388	0.7487	0.009	0.1013	-0.8047
	Preoperative factors	Altered fetal cerebral substrate delivery	-0.4349	-0.2581	0.784	0.2262	0.3117
Altered fetal substrate delivery, severity score		-0.0559	-0.2424	-0.4373	0.0731	0.3005	0.751
Heterotaxy		0.3437	0.4249	0.577	-0.9005	-0.7657	-0.7109
Preoperative arterial blood gas pH		-0.0444	-0.0532	-0.128	0.2902	0.6587	0.8897
Preoperative arterial blood gas pO2		0.7139	0.1438	0.8756	-0.6411	0.6388	-0.2578
Preoperative arterial lactate		0.609	0.6729	0.4887	0.9987	0.4399	-0.2661
Preoperative hepatic dysfunction		0.1413	0.2046	0.1575	0.8789	0.8958	0.8389
Preoperative inotrope use		-0.6446	-0.1852	-0.6888	-0.967	-0.0832	-0.4767
Age at surgery, days		0.5973	0.4562	0.3746	0.1595	0.6875	-0.4308
Post-conceptual age at surgery, weeks		0.473	0.3836	0.6587	0.2224	0.9365	-0.5161
Intraoperative factors	Cardiopulmonary bypass used	-0.6136	-0.737	-0.66	-0.864	0.7605	-0.1917
	Cardiopulmonary bypass time	-0.4517	-0.5571	-0.1952	0.4127	-0.593	-0.5451
	Aortic cross-clamp used	-0.8278	-0.7459	-0.4735	-0.16	-0.8284	-0.2995
	Aortic cross-clamp time	-0.8423	-0.9097	-0.4466	0.8169	-0.3826	-0.524
	Circulatory arrest/DHCA used	-0.7393	0.671	0.4861	-0.8968	0.165	-0.0051
	Circulatory arrest/DHCA time	-0.418	-0.861	0.8306	0.8215	0.031	-0.1187
	ECMO during 1 st hospitalization	-0.9575	-0.6103	-0.7278	-0.2475	-0.088	-0.827
	Time on ECMO (days)	-0.4635	-0.3165	-0.4087	-0.4905	-0.2352	-0.7835
	Delayed sternal closure	-0.9673	0.4216	0.8002	0.6009	0.4257	-0.4587
	Had unplanned intervention(s), 1 st hospitalization	-0.8938	-0.7	-0.3149	-0.7572	-0.1424	-0.8704
Postoperative factors	ICU length of stay, 1 st hospitalization	-0.7763	-0.6725	-0.4364	-0.9797	-0.6921	0.9291
	Hospital length of stay	-0.5218	-0.6434	-0.246	0.8926	-0.8239	-0.779
	Expired during 1 st hospitalization	-0.5742	-0.3424	-0.5219	0.9913	-0.4949	0.9834
	Required CPR during 1 st hospitalization	0.6693	-0.9399	-0.4697	-0.1615	-0.2419	0.7517
	Had seizures during 1 st hospitalization	-0.0388	-0.0714	-0.0704	0.1237	0.3648	-0.7843
	Discharged on antiepileptics	0.8048	0.4454	-0.6969	0.9339	0.4292	-0.7385
	Discharged with gastrostomy tube	0.9248	-0.9773	-0.1932	-0.3559	-0.1179	0.1806
	Discharged with tracheostomy and/or ventilator	-0.215	-0.6838	-0.4707	0.6231	0.1736	-0.833

855 TGA = transposition of the great arteries, CPR=cardiopulmonary resuscitation, DHCA=deep hypothermic circulatory arrest, ECMO=extra
 856 corporeal membrane oxygenation, ICU=intensive care unit

857 **Table 2(B). Correlation Between Clinical Risk Factors and Global Connectome Metrics: Number of Tracts Matrix (FDR-corrected)**

		Cost	Global Efficiency	Transitivity	Modularity	Small World	Assortativity
Innate and cardiac lesions	Gestational age at birth	0.2918	0.1846	0.524	-0.5181	0.4814	-0.7608
	Birth weight	0.9739	0.6472	0.6176	-0.2367	0.0759	-0.9972
	Birth weight percentile	-0.299	-0.3999	-0.8739	-0.8968	0.0725	0.2328
	Head circumference	0.2385	0.2246	0.4581	-0.5984	0.8289	-0.5454
	Head circumference percentile	0.7785	1	0.429	-0.7041	0.1823	0.7831
	Birth length	0.3057	0.2915	-0.8689	-0.5285	-0.2581	-0.8874
	Birth length percentile	0.1748	0.2791	0.7156	-0.2275	-0.12	0.0565
	APGAR, 1 minute	-0.9608	0.4852	-0.6635	-0.2196	0.4353	-0.334
	APGAR, 5 minute	-0.7745	0.7962	0.9329	-0.5814	0.6284	-0.8021
	22q11 microdeletion	0.3997	0.4856	0.7645	-0.5744	0.9477	0.9463
	Single ventricle	0.0825	0.1872	0.1694	-0.2159	-0.1002	0.8596
	Arch obstruction	0.575	0.6645	0.8957	-0.0098	-0.0361	0.2608
	Single ventricle with arch obstruction	0.1453	0.3584	0.1226	-0.4095	-0.1829	0.1547
	d-TGA	-0.0043	-0.0058	-0.0203	0.0435	0.101	0.8169
	Conotruncal defect	-0.5529	-0.4627	-0.7289	0.0111	0.2363	-0.8047
Preoperative factors	Altered fetal cerebral substrate delivery	-0.458	-0.2826	-0.8858	0.1006	0.3929	-0.4175
	Altered cerebral substrate delivery severity score	-0.0073	-0.0054	-0.046	0.0585	0.3361	0.751
	Heterotaxy	0.1544	0.1302	0.3229	-0.6267	-0.3342	-0.7109
	Preoperative arterial blood gas pH	-0.1056	-0.0875	-0.0558	0.5133	0.7699	0.8897
	Preoperative arterial blood gas pO2	0.8971	0.5152	0.8042	-0.6566	0.5429	-0.2578
	Preoperative arterial lactate	0.8769	0.9856	0.8261	0.4515	-0.8143	-0.2661
	Preoperative hepatic dysfunction	0.8081	0.9093	0.8589	0.8398	-0.9418	0.8389
	Preoperative inotrope use	-0.6951	-0.4534	-0.562	0.8415	-0.1463	-0.4767
	Age at surgery, days	0.9474	-0.8745	-0.9641	0.3906	-0.5035	-0.4308
	Age at surgery ≤7 days	0.9424	0.8055	0.455	-0.5178	0.1021	0.9782
	Post-conceptional age at surgery, weeks	0.607	0.5579	0.8236	0.9837	0.9641	-0.5161
	Cardiopulmonary bypass used	-0.1086	-0.1435	-0.3265	0.187	0.3983	-0.1917
	Cardiopulmonary bypass time	-0.0759	-0.0765	-0.0663	-0.9521	-0.6056	-0.5451
	Aortic cross-clamp used	-0.1836	-0.2674	-0.1699	0.2248	0.5837	-0.2995
	Aortic cross-clamp time	-0.5709	-0.5751	-0.5269	-0.9326	-0.671	-0.524
Circulatory arrest/DHCA used	-0.9488	0.8619	0.6678	-0.5385	0.6901	-0.0051	
Circulatory arrest/DHCA time	-0.8855	0.9394	0.6792	-0.9018	0.2848	-0.1187	
Postoperative factors	ECMO during 1 st hospitalization	-0.3713	-0.2622	-0.2767	-0.6661	-0.0545	-0.827
	Time on ECMO (days)	-0.1446	-0.1052	-0.0973	0.9931	-0.0878	-0.7835
	Delayed sternal closure	-0.5379	-0.6143	-0.6814	0.3623	0.9183	-0.4587
	Had unplanned intervention(s), 1 st hospitalization	-0.3879	-0.3596	-0.1475	-0.6329	-0.0733	-0.8704
	ICU length of stay, 1 st hospitalization	-0.6355	-0.5327	-0.3574	-0.3949	-0.2001	0.9291
	Hospital length of stay	-0.3037	-0.283	-0.1566	-0.448	-0.1779	-0.779
	Expired during 1 st hospitalization	-0.6103	-0.4601	-0.3885	-0.194	-0.1493	0.9834
	Required CPR during 1 st hospitalization	-0.7533	-0.5378	-0.3742	-0.1507	-0.1666	0.7517
	Had seizures during 1 st hospitalization	-0.1804	-0.1351	-0.1467	0.279	-0.8936	-0.7843
	Discharged on antiepileptics	-0.9114	-0.8641	-0.8618	0.3822	0.5556	-0.7385
	Discharged with gastrostomy tube	-0.5563	-0.6523	-0.1695	0.9847	-0.3562	0.1806
	Discharged with tracheostomy and/or ventilator	-0.0674	-0.1208	-0.1959	0.1477	0.3242	-0.833

858 TGA = transposition of the great arteries, CPR=cardiopulmonary resuscitation, DHCA=deep hypothermic circulatory arrest, ECMO=extra
859 corporeal membrane oxygenation, ICU=intensive care unit

860 Table 2(C). Correlation Between Clinical Risk Factors and Global Connectome Metrics: Average Fractional Anisotropy Matrix (FDR-
861 corrected)

		Cost	Global Efficiency	Transitivity	Modularity	Small World	Assortativity
Innate and cardiac lesions	Gestational age at birth	0.2129	0.2726	0.6258	-0.938	-0.9175	-0.7608
	Birth weight	-0.7891	-0.9483	-0.8389	0.6793	0.9634	-0.9972
	Birth weight percentile	-0.2619	-0.3833	-0.7516	0.0946	0.2292	0.2328
	Head circumference	0.7205	0.9823	0.8313	0.8605	0.9079	-0.5454
	Head circumference percentile	-0.5598	-0.2367	0.8029	0.4178	0.192	0.7831
	Birth length	0.7429	0.856	-0.6331	-0.6738	-0.3599	-0.8874
	Birth length percentile	0.9289	-0.7633	-0.47	-0.2075	-0.2277	0.0565
	APGAR, 1 minute	-0.6998	0.6338	-0.3445	-0.4049	-0.8701	-0.334
	APGAR, 5 minute	0.6623	0.3672	0.3478	-0.4664	0.6321	-0.8021
	22q11 microdeletion	-0.1672	-0.1146	-0.2041	-0.8494	-0.8558	0.9463
	Single ventricle	0.2122	0.918	0.6752	-0.0998	-0.1202	0.8596
	Arch obstruction	0.4403	0.8931	-0.6476	-0.0183	-0.0039	0.2608
	Single ventricle with arch obstruction	0.8128	-0.4546	-0.9548	-0.1547	-0.1898	0.1547
	d-TGA	-0.1558	-0.4273	-0.7334	0.0237	0.0353	0.8169
	Conotruncal defect	-0.2603	-0.3807	0.8804	0.0075	0.0305	-0.8047
	Altered fetal cerebral substrate delivery	-0.2248	-0.1727	-0.7726	0.3247	0.1395	-0.4175
Altered cerebral substrate delivery severity score	-0.1602	-0.4154	-0.7166	0.1529	0.1429	0.751	
Heterotaxy	0.4118	0.5625	0.55	0.6015	-0.6252	-0.7109	
Preoperative factors	Preoperative arterial blood gas pH	-0.1064	-0.1201	-0.2402	0.5332	0.7033	0.8897
	Preoperative arterial blood gas pO2	-0.8363	0.5042	-0.5876	-0.789	0.7652	-0.2578
	Preoperative arterial lactate	0.722	0.7662	0.5436	-0.9811	0.2692	-0.2661
	Preoperative hepatic dysfunction	0.8424	0.9009	0.8052	-0.7401	0.6648	0.8389
	Preoperative inotrope use	-0.2349	-0.0956	-0.2937	-0.7737	-0.128	-0.4767
	Age at surgery, days	0.7364	0.6158	0.544	0.1907	-0.9121	-0.4308
	Age at surgery ≤7 days	-0.9697	-0.8198	0.7901	-0.5234	0.307	0.9782
	Post-conceptual age at surgery, weeks	0.2976	0.2375	0.3806	0.3008	0.9289	-0.5161
Intraoperative factors	Cardiopulmonary bypass used	-0.1915	-0.2437	-0.2629	-0.5077	0.5177	-0.1917
	Cardiopulmonary bypass time	-0.0271	-0.0373	-0.0173	0.8561	-0.9387	-0.5451
	Aortic cross-clamp used	-0.4251	-0.4333	-0.2282	-0.1459	0.9109	-0.2995
	Aortic cross-clamp time	-0.192	-0.2131	-0.0727	0.6495	-0.4238	-0.524
	Circulatory arrest/DHCA used	-0.6456	0.8999	0.6391	-0.3985	0.2857	-0.0051
	Circulatory arrest/DHCA time	-0.594	-0.9883	0.7047	-0.7415	0.0247	-0.1187
Postoperative factors	ECMO during 1 st hospitalization	-0.193	-0.0566	-0.2699	-0.1254	-0.1765	-0.827
	Time on ECMO (days)	-0.0404	-0.0116	-0.0938	-0.2941	-0.379	-0.7835
	Delayed sternal closure	-0.9928	0.4595	0.6821	-0.5052	0.5109	-0.4587
	Had unplanned intervention(s), 1 st hospitalization	-0.2819	-0.16	-0.2036	-0.4477	-0.3391	-0.8704
	ICU length of stay, 1 st hospitalization	-0.2399	-0.1934	-0.2395	-0.9562	-0.898	0.9291
	Hospital length of stay	-0.166	-0.2456	-0.1726	0.8774	0.9816	-0.779
	Expired during 1 st hospitalization	-0.0926	-0.0318	-0.1541	0.6219	-0.6581	0.9834
	Required CPR during 1 st hospitalization	-0.2268	-0.0361	-0.0608	-0.7409	-0.2031	0.7517
	Had seizures during 1 st hospitalization	-0.0496	-0.0908	-0.1527	0.2009	0.4436	-0.7843
	Discharged on antiepileptics	-0.9194	0.9117	-0.6587	-0.9203	0.8254	-0.7385
	Discharged with gastrostomy tube	-0.8844	-0.8286	-0.2652	-0.257	-0.1839	0.1806
Discharged with tracheostomy and/or ventilator	-0.1789	-0.4994	-0.4402	-0.7227	0.2231	-0.833	

862 TGA = transposition of the great arteries, CPR=cardiopulmonary resuscitation, DHCA=deep hypothermic circulatory arrest, ECMO=extra
863 corporeal membrane oxygenation, ICU=intensive care unit

864 **Table 3. Correlation Between Subcortical Brain Dysplasia Score (BDS), Brain Injury and Global Connectome Metrics (FDR-corrected)**

		Cost	Global Efficiency	Transitivity	Modularity	Small World	Assortativity
Adjacency Matrix, Preoperative MRI	BDS	-0.0817	-0.0525	-0.1839	0.1353	0.218	-0.6677
	Cerebellum	-0.0417	-0.2953	-0.2506	0.5293	0.1854	-0.3837
	Olfactory	-0.6433	-0.7436	-0.8967	0.0766	0.1612	-0.3406
	Hippocampal	-0.1005	-0.0126	-0.0776	0.3526	0.9879	0.1771
	Brain Injury	-0.0773	-0.0936	-0.2051	0.1927	0.9104	0.6224
	Stroke	0.7366	-0.8034	-0.5851	-0.6983	-0.4022	-0.3788
	Punctate white mater injury	-0.0401	-0.0552	-0.1822	0.2154	-0.7936	0.1389
Adjacency Matrix, Postoperative MRI	BDS	0.1183	0.0806	0.1422	0.3276	-0.1717	-0.4248
	Cerebellum	0.3625	0.3195	0.1936	-0.9118	-0.4835	-0.1075
	Olfactory	0.137	0.0916	0.0663	0.2404	-0.323	-0.393
	Hippocampal	0.3582	0.4186	-0.9307	0.3746	-0.0616	-0.8561
	Brain Injury	-0.2206	-0.204	-0.2319	0.1666	0.284	0.6022
	Stroke	-0.0437	-0.0285	-0.0439	0.2592	0.8144	0.0381
	Punctate white mater injury	-0.7189	-0.6146	-0.4661	0.2569	0.6579	-0.6747
Number of Tracts Matrix, Preoperative MRI	BDS	-0.4672	-0.3245	-0.7039	0.0846	0.4401	-0.6677
	Cerebellum	-0.0117	-0.0467	-0.0762	-0.9661	0.1175	-0.3837
	Olfactory	0.6876	0.8216	0.4707	0.021	0.2736	-0.3406
	Hippocampal	-0.4156	-0.2242	-0.2342	0.997	-0.4147	0.1771
	Brain Injury	-0.2819	-0.3661	-0.5621	0.7756	0.3986	0.6224
	Stroke	0.4722	0.4767	0.7012	-0.1498	-0.8963	-0.3788
	Punctate white mater injury	-0.1582	-0.2679	-0.344	0.8958	0.5207	0.1389
Number of Tracts Matrix, Postoperative MRI	BDS	0.1484	0.2503	0.1179	-0.8474	-0.3386	-0.4248
	Cerebellum	0.0567	0.0654	0.0697	-0.2503	-0.5315	-0.1075
	Olfactory	0.3392	0.4785	0.181	0.488	-0.613	-0.393
	Hippocampal	0.1894	0.2657	0.231	-0.1688	-0.2635	-0.8561
	Brain Injury	-0.0988	-0.0615	-0.1599	-0.9669	0.4344	0.6022
	Stroke	-0.3329	-0.4203	-0.0995	-0.7676	0.5287	0.0381
	Punctate white mater injury	-0.5409	-0.4706	-0.5737	-1	0.8858	-0.6747
Average Fractional Anisotropy Preoperative MRI	BDS	-0.5744	-0.544	-0.6988	0.4685	0.1233	-0.6677
	Cerebellum	-0.0388	-0.2154	-0.2026	0.5875	0.1404	-0.3837
	Olfactory	0.5741	0.4828	0.5078	0.4721	0.1548	-0.3406
	Hippocampal	-0.3403	-0.118	-0.2409	0.4253	0.9481	0.1771
	Brain Injury	-0.2765	-0.3748	-0.445	0.5613	-0.8481	0.6224
	Stroke	0.9845	-0.6852	-0.5091	-0.72	-0.1931	-0.3788
	Punctate white matter injury	-0.1288	-0.2154	-0.3457	0.5821	-0.694	0.1389
Average Fractional Anisotropy Postoperative MRI	BDS	0.4757	0.5487	0.3432	0.7551	-0.2918	-0.4248
	Cerebellum	0.4413	0.5061	0.1702	-0.8609	-0.7585	-0.1075
	Olfactory	0.3753	0.394	0.1805	0.6156	-0.4073	-0.393
	Hippocampal	-0.6546	-0.3959	-0.3226	0.796	-0.1053	-0.8561
	Brain Injury	-0.0994	-0.1034	-0.1698	0.365	0.3303	0.6022
	Stroke	-0.1593	-0.1399	-0.1677	0.2267	0.9753	0.0381
	Punctate white matter injury	-0.6274	-0.5925	-0.5907	0.3855	0.7528	-0.6747

865 MRI = Magnetic Resonance Imaging, BDS = Brain Dysplasia Score

866 **Table 4. Correlation Between Brain Dysplasia Score (BDS) (including subcortical components) and Seed-based Tractography Metrics**
867 (FDR-corrected)

		Fractional Anisotropy			Radial Diffusivity			Axial Diffusivity		
		Pre	Post	All	Pre	Post	All	Pre	Post	All
Corpus Callosum Genu	BDS	0.0489	0.6865	0.1426	0.0029	0.8118	0.025	0.0194	0.8855	0.2067
	Cerebellum	0.4839	0.5308	0.9382	0.0275	0.6841	0.1982	0.0251	0.7969	0.1702
	Olfactory	0.2686	0.9773	0.4723	0.2837	0.6018	0.5085	0.7493	0.7435	0.9642
	Hippocampal	0.2468	0.8402	0.6056	0.0133	0.5037	0.0282	0.0212	0.5277	0.061
Corpus Callosum Body	BDS	0.2271	0.5468	0.2399	0.0173	0.8118	0.0921	0.0371	0.782	0.3028
	Cerebellum	0.4581	0.9952	0.6303	0.0391	0.6841	0.1746	0.0947	0.6346	0.3295
	Olfactory	0.8371	0.7989	0.7452	0.9785	0.6018	0.6941	0.9095	0.6089	0.7182
	Hippocampal	0.1839	0.8296	0.3511	0.0002	0.5037	0.0029	0.0005	0.7277	0.0122
Corpus Callosum Splenium	BDS	0.1747	0.9669	0.3038	0.002	0.7703	0.0086	0.0029	0.8771	0.0262
	Cerebellum	0.4251	0.7146	0.6587	<0.0001	0.7349	0.0004	<0.0001	0.8891	0.0004
	Olfactory	0.3839	0.9184	0.5273	0.3568	0.8085	0.4968	0.3885	0.7682	0.6243
	Hippocampal	0.3557	0.7932	0.6366	0.0004	0.2667	0.0005	0.0003	0.2483	0.0007
Cortical Spinal Tract Left	BDS	0.5901	0.9105	0.5348	0.9743	0.4924	0.6447	0.8467	0.4859	0.4524
	Cerebellum	0.0826	0.1654	0.0223	0.9191	0.9768	0.9458	0.4199	0.5598	0.2825
	Olfactory	0.7273	0.564	0.4249	0.4553	0.6249	0.7845	0.3632	0.3673	0.9907
	Hippocampal	0.3988	0.6435	0.3048	0.4696	0.3219	0.2178	0.1532	0.1974	0.0428
Cortical Spinal Tract Right	BDS	0.1017	0.4165	0.0495	0.6399	0.83	0.8542	0.8008	0.5668	0.4538
	Cerebellum	0.0288	0.0601	0.0036	0.8618	0.6913	0.7149	0.4189	0.6118	0.304
	Olfactory	0.2036	0.4406	0.1241	0.1285	0.8603	0.2518	0.2291	0.5701	0.5722
	Hippocampal	0.2161	0.3139	0.086	0.4347	0.9691	0.5279	0.1214	0.6186	0.1152
Fronto-occipital Fasciculus Left	BDS	0.13	0.719	0.5897	0.0415	0.4147	0.5228	0.0766	0.3593	0.7491
	Cerebellum	0.1437	0.4141	0.6858	0.2875	0.8409	0.5211	0.701	0.7798	0.6798
	Olfactory	0.8631	0.4291	0.6268	0.5179	0.3852	0.8711	0.4226	0.6026	0.885
	Hippocampal	0.1234	0.6281	0.6567	0.0034	0.4102	0.246	0.006*	0.3129	0.4062
Fronto-occipital Fasciculus Right	BDS	0.5517	0.4682	0.6938	0.1853	0.209	0.8943	0.1579	0.203	0.9817
	Cerebellum	0.4365	0.7093	0.8125	0.0459	0.7901	0.1887	0.0495*	0.9664	0.1502
	Olfactory	0.7617	0.3383	0.3335	0.9519	0.1469	0.296	0.8176	0.156	0.4367
	Hippocampal	0.293	0.3687	0.8473	0.1328	0.1471	0.8483	0.1997	0.0976	0.6319
Inferior Longitudinal Fasciculus Left	BDS	0.1906	0.9454	0.2937	0.018	0.1219	0.0044	0.0464	0.1557	0.0127
	Cerebellum	0.6072	0.2079	0.8331	0.0287	0.1928	0.0088	0.0422	0.0869	0.007
	Olfactory	0.7237	0.6934	0.6289	0.2189	0.1329	0.0548	0.2429	0.1469	0.0638
	Hippocampal	0.3554	0.9786	0.7845	0.0054	0.4265	0.0082	0.0082	0.4136	0.0109
Inferior Longitudinal Fasciculus Right	BDS	0.2306	0.4673	0.5476	0.1753	0.9759	0.281	0.2829	0.9581	0.4614
	Cerebellum	0.5603	0.7997	0.8938	0.4044	0.9935	0.4452	0.5562	0.5805	0.4227
	Olfactory	0.6648	0.7904	0.8086	0.3863	0.9766	0.4474	0.366	0.7085	0.3456
	Hippocampal	0.1477	0.7262	0.4223	0.0635	0.8869	0.123	0.1317	0.9192	0.2955
Superior Longitudinal Fasciculus Left	BDS	0.0788	0.4744	0.1092	0.3259	0.8205	0.5096	0.6847	0.4671	0.9068
	Cerebellum	0.9084	0.3257	0.9145	0.888	0.1867	0.441	0.8351	0.2193	0.4204
	Olfactory	0.283	0.2389	0.3002	0.783	0.9614	0.836	0.9008	0.8025	0.8044
	Hippocampal	0.1171	0.2793	0.4844	0.2186	0.4673	0.1552	0.4839	0.5139	0.3374
Superior Longitudinal Fasciculus Right	BDS	0.9582	0.9454	0.5138	0.5083	0.3462	0.7487	0.3416	0.3821	0.81
	Cerebellum	0.7902	0.2079	0.413	0.3184	0.2997	0.8822	0.1067	0.6421	0.4454
	Olfactory	0.386	0.6934	0.1821	0.5341	0.3417	0.255	0.8247	0.5582	0.5314
	Hippocampal	0.4305	0.9786	0.6757	0.0449	0.8933	0.1611	0.0263	0.7581	0.1362

868 BDS = Brain Dysplasia Score

869 **REFERENCES**

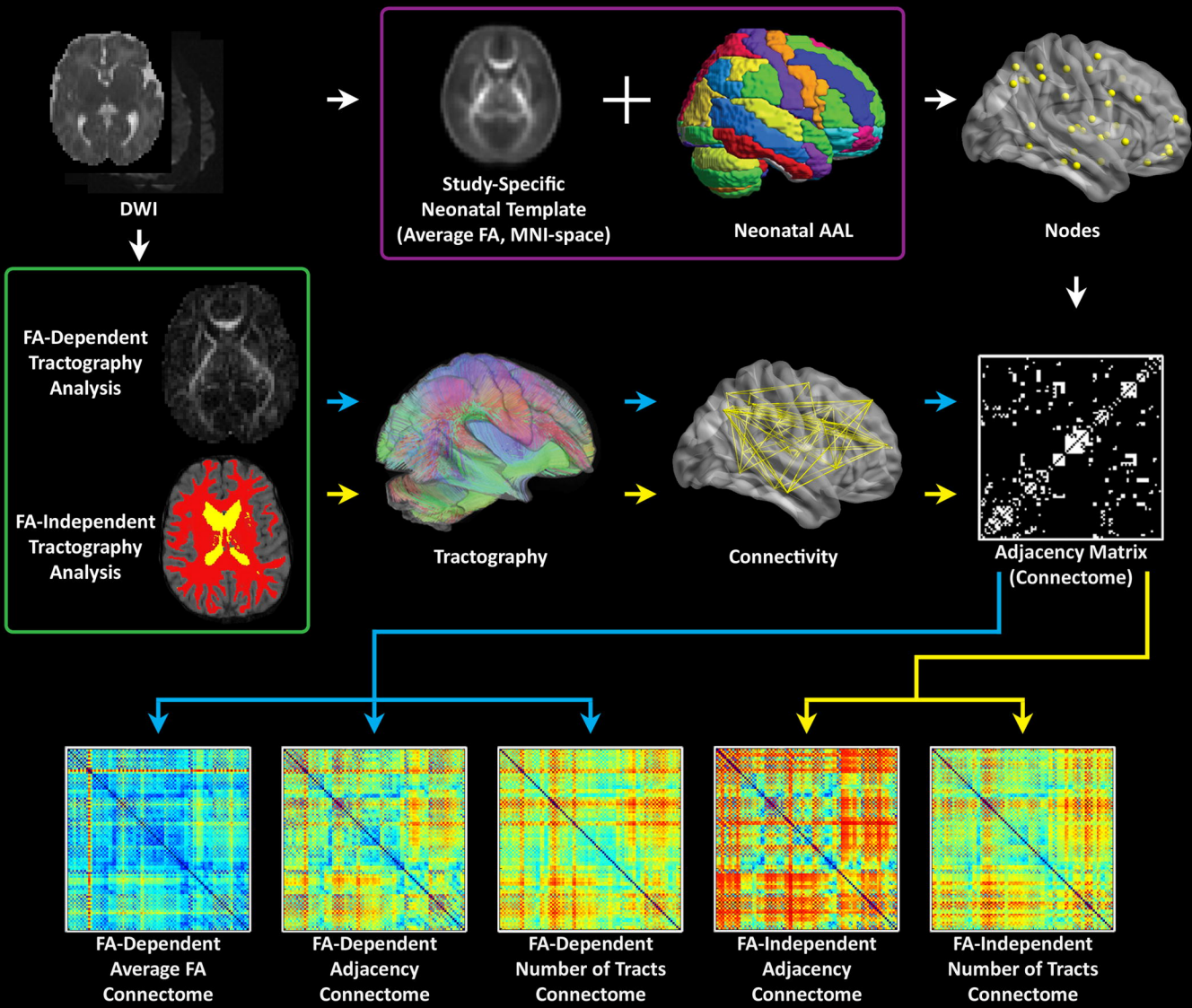
- 870 1. van der Linde D, Konings EE, Slager MA, et al. Birth prevalence of congenital heart disease
871 worldwide: a systematic review and meta-analysis. *Meta-Analysis*
872 *Review. Journal of the American College of Cardiology*. Nov 15 2011;58(21):2241-7.
873 doi:10.1016/j.jacc.2011.08.025
- 874 2. Marino BS, Lipkin PH, Newburger JW, et al. Neurodevelopmental outcomes in children with
875 congenital heart disease: evaluation and management: a scientific statement from the American Heart
876 Association. Practice Guideline. *Circulation*. Aug 28 2012;126(9):1143-72.
877 doi:10.1161/CIR.0b013e318265ee8a
- 878 3. Gaynor JW, Stopp C, Wypij D, et al. Neurodevelopmental outcomes after cardiac surgery in
879 infancy. Research Support, N.I.H., Extramural
880 Research Support, Non-U.S. Gov't. *Pediatrics*. May 2015;135(5):816-25. doi:10.1542/peds.2014-3825
- 881 4. Bellinger DC, Newburger JW, Wypij D, Kuban KC, duPlessis AJ, Rappaport LA. Behaviour at eight
882 years in children with surgically corrected transposition: The Boston Circulatory Arrest Trial. *Cardiol*
883 *Young*. Feb 2009;19(1):86-97. doi:10.1017/s1047951108003454
- 884 5. Pike NA, Woo MA, Poulsen MK, et al. Predictors of Memory Deficits in Adolescents and Young
885 Adults with Congenital Heart Disease Compared to Healthy Controls. *Frontiers in pediatrics*. 2016;4:117.
886 doi:10.3389/fped.2016.00117
- 887 6. Cassidy AR, White MT, DeMaso DR, Newburger JW, Bellinger DC. Executive Function in Children
888 and Adolescents with Critical Cyanotic Congenital Heart Disease. Research Support, N.I.H., Extramural
889 Research Support, Non-U.S. Gov't. *Journal of the International Neuropsychological Society : JINS*. Jan
890 2015;21(1):34-49. doi:10.1017/S1355617714001027
- 891 7. Mussatto KA, Hoffmann RG, Hoffman GM, et al. Risk and prevalence of developmental delay in
892 young children with congenital heart disease. Research Support, N.I.H., Extramural. *Pediatrics*. Mar
893 2014;133(3):e570-7. doi:10.1542/peds.2013-2309
- 894 8. Miller SP, McQuillen PS, Hamrick S, et al. Abnormal brain development in newborns with
895 congenital heart disease. Research Support, N.I.H., Extramural
896 Research Support, Non-U.S. Gov't. *The New England journal of medicine*. Nov 8 2007;357(19):1928-38.
897 doi:10.1056/NEJMoa067393
- 898 9. Licht DJ, M. SD, R. CR, et al. Brain maturation is delayed in infants with complex congenital heart
899 defects. *The Journal of thoracic and cardiovascular surgery*. 2009;137(3):529--36; discussion 536--7.
900 doi:10.1016/j.jtcvs.2008.10.025
- 901 10. Panigrahy A, Lee V, Ceschin R, et al. Brain Dysplasia Associated with Ciliary Dysfunction in Infants
902 with Congenital Heart Disease. *The Journal of pediatrics*. 2016;
- 903 11. Limperopoulos C, Tworetzky W, McElhinney DB, et al. Brain volume and metabolism in fetuses
904 with congenital heart disease: evaluation with quantitative magnetic resonance imaging and
905 spectroscopy. Research Support, N.I.H., Extramural
906 Research Support, Non-U.S. Gov't. *Circulation*. Jan 5 2010;121(1):26-33.
907 doi:10.1161/CIRCULATIONAHA.109.865568
- 908 12. Rajagopalan V, Votava-Smith JK, Zhuang X, et al. Fetuses with single ventricle congenital heart
909 disease manifest impairment of regional brain growth. *Prenatal diagnosis*. Dec 2018;38(13):1042-1048.
910 doi:10.1002/pd.5374
- 911 13. Sun L, Macgowan CK, Sled JG, et al. Reduced fetal cerebral oxygen consumption is associated
912 with smaller brain size in fetuses with congenital heart disease. Observational Study
913 Research Support, N.I.H., Extramural. *Circulation*. Apr 14 2015;131(15):1313-23.
914 doi:10.1161/CIRCULATIONAHA.114.013051

- 915 14. Beca J, Gunn JK, Coleman L, et al. New white matter brain injury after infant heart surgery is
916 associated with diagnostic group and the use of circulatory arrest. *Circulation*. Mar 5 2013;127(9):971-9.
917 doi:10.1161/circulationaha.112.001089
- 918 15. Rollins CK, Watson CG, Asaro LA, et al. White matter microstructure and cognition in
919 adolescents with congenital heart disease. Research Support, N.I.H., Extramural
920 Research Support, Non-U.S. Gov't. *The Journal of pediatrics*. Nov 2014;165(5):936-44 e1-2.
921 doi:10.1016/j.jpeds.2014.07.028
- 922 16. Panigrahy A, Schmithorst VJ, Wisnowski JL, et al. Relationship of white matter network topology
923 and cognitive outcome in adolescents with d-transposition of the great arteries. *NeuroImage: Clinical*.
924 2015;7:438-448.
- 925 17. Bhroin MN, Seada SA, Bonthron AF, et al. Reduced structural connectivity in cortico-striatal-
926 thalamic network in neonates with congenital heart disease. *NeuroImage: Clinical*. 2020;28:102423.
- 927 18. Feldmann M, Guo T, Miller SP, et al. Delayed maturation of the structural brain connectome in
928 neonates with congenital heart disease. *Brain communications*. 2020;2(2):fcaa209.
- 929 19. Ji W, Ferdman D, Copel J, et al. De novo damaging variants associated with congenital heart
930 diseases contribute to the connectome. *Scientific reports*. 2020;10(1):1-11.
- 931 20. Ramirez A, Peyvandi S, Cox S, et al. Neonatal brain injury influences structural connectivity and
932 childhood functional outcomes. *PLoS one*. 2022;17(1):e0262310.
- 933 21. Schmithorst VJ, Votava-Smith JK, Tran N, et al. Structural network topology correlates of
934 microstructural brain dysmaturation in term infants with congenital heart disease. *Human brain
935 mapping*. 2018;39(11):4593-4610.
- 936 22. Brambrink AM, Evers AS, Avidan MS, et al. Isoflurane-induced neuroapoptosis in the neonatal
937 rhesus macaque brain. *Anesthesiology: The Journal of the American Society of Anesthesiologists*.
938 2010;112(4):834-841.
- 939 23. Brambrink AM, Back SA, Riddle A, et al. Isoflurane-induced apoptosis of oligodendrocytes in the
940 neonatal primate brain. *Annals of neurology*. 2012;72(4):525-535.
- 941 24. Block AJ, McQuillen PS, Chau V, et al. Clinically silent preoperative brain injuries do not worsen
942 with surgery in neonates with congenital heart disease. *J Thorac Cardiovasc Surg*. Sep 2010;140(3):550-
943 7. doi:10.1016/j.jtcvs.2010.03.035
- 944 25. McQuillen PS, P. MS. Congenital heart disease and brain development. *Annals of the New York
945 Academy of Sciences*. 2010;1184:68--86. doi:10.1111/j.1749-6632.2009.05116.x
- 946 26. Gaynor JW, Stopp C, Wypij D, et al. Impact of operative and postoperative factors on
947 neurodevelopmental outcomes after cardiac operations. *The Annals of Thoracic Surgery*.
948 2016;102(3):843-849.
- 949 27. Beca J, Gunn J, Coleman L, et al. Pre-operative brain injury in newborn infants with transposition
950 of the great arteries occurs at rates similar to other complex congenital heart disease and is not related
951 to balloon atrial septostomy. *J Am Coll Cardiol*. May 12 2009;53(19):1807-11.
952 doi:10.1016/j.jacc.2009.01.061
- 953 28. Petit CJ, Rome JJ, Wernovsky G, et al. Preoperative brain injury in transposition of the great
954 arteries is associated with oxygenation and time to surgery, not balloon atrial septostomy. *Circulation*.
955 Feb 10 2009;119(5):709-16. doi:10.1161/circulationaha.107.760819
- 956 29. Peyvandi S, Latal B, Miller SP, McQuillen PS. The neonatal brain in critical congenital heart
957 disease: insights and future directions. *NeuroImage*. 2019;185:776-782.
- 958 30. Ceschin R, Zahner A, Reynolds W, et al. A computational framework for the detection of
959 subcortical brain dysmaturation in neonatal MRI using 3D Convolutional Neural Networks. *NeuroImage*.
960 2018;178:183-197.

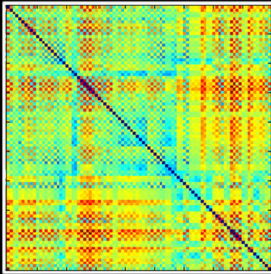
- 961 31. Gabriel GC, Salamacha N, Reynolds WT, et al. Characterization of Neurodevelopmental Defects
962 Associated With a Mouse Model of Hypoplastic Left Heart Syndrome. *Circulation*.
963 2018;138(Suppl_1):A16609-A16609.
- 964 32. Panigrahy A, Ceschin R, Lee V, et al. Respiratory Ciliary Motion Defect Predict Regional Brain
965 Abnormalities and Increased Extra Axial CSF Fluid in Neonates With Complex Congenital Heart Disease.
966 *Circulation*. 2014;130(suppl_2):A16570-A16570.
- 967 33. Panigrahy A, Votava-Smith J, Lee V, et al. Abnormal Brain Connectivity and Poor
968 Neurodevelopmental Outcome in Congenital Heart Disease Patients With Subtle Brain Dysplasia.
969 *Circulation*. 2015;132(suppl_3):A16541-A16541.
- 970 34. Subramanian S, Soundara Rajan D, Gaesser J, Wen-Ya Lo C, Panigrahy A. Olfactory bulb and
971 olfactory tract abnormalities in acrocallosal syndrome and Greig cephalopolysyndactyly syndrome.
972 *Pediatric radiology*. 2019;49(10):1368-1373.
- 973 35. Votava-Smith JK, Tran N, Abbott J, et al. Impaired Cerebral Autoregulation is Associated With
974 Brain Abnormalities in Neonatal Congenital Heart Disease: Initial Experience. *Circulation*.
975 2016;134(suppl_1):A18081-A18081.
- 976 36. Jenkins KJ, Gauvreau K, Newburger JW, Spray TL, Moller JH, Iezzoni LI. Consensus-based method
977 for risk adjustment for surgery for congenital heart disease. *J Thorac Cardiovasc Surg*. Jan
978 2002;123(1):110-8.
- 979 37. Mahle WT, Tavani F, Zimmerman RA, et al. An MRI study of neurological injury before and after
980 congenital heart surgery. *Clinical Trial*
981 Research Support, Non-U.S. Gov't. *Circulation*. Sep 24 2002;106(12 Suppl 1):I109-14.
- 982 38. Limperopoulos C, Majnemer A, Shevell MI, et al. Predictors of developmental disabilities after
983 open heart surgery in young children with congenital heart defects. *J Pediatr*. Jul 2002;141(1):51-8.
984 doi:10.1067/mpd.2002.125227
- 985 39. Shi F, Yap PT, Wu G, et al. Infant brain atlases from neonates to 1- and 2-year-olds. Research
986 Support, N.I.H., Extramural. *PLoS one*. 2011;6(4):e18746. doi:10.1371/journal.pone.0018746
- 987 40. Alcauter S, Lin W, Smith JK, Gilmore JH, Gao W. Consistent anterior-posterior segregation of the
988 insula during the first 2 years of life. *Cereb Cortex*. 2015;25(5):1176-1187.
- 989 41. Gao W, Alcauter S, Smith JK, Gilmore JH, Lin W. Development of human brain cortical network
990 architecture during infancy. *Brain Structure and Function*. 2014;220(2):1173-1186.
- 991 42. Thomason ME, Brown JA, Dassanayake MT, et al. Intrinsic functional brain architecture derived
992 from graph theoretical analysis in the human fetus. *PLoS one*. 2014;9(5):e94423.
- 993 43. Thomason ME, Grove LE, Lozon TA, et al. Age-related increases in long-range connectivity in
994 fetal functional neural connectivity networks in utero. *Developmental cognitive neuroscience*.
995 2015;11:96-104.
- 996 44. Menon V. Large-scale brain networks and psychopathology: a unifying triple network model.
997 *Trends Cogn Sci*. 2011;15(10):483-506.
- 998 45. Gao W, Gilmore JH, Giovanello KS, et al. Temporal and spatial evolution of brain network
999 topology during the first two years of life. *PLoS one*. 2011;6(9):e25278.
- 1000 46. Gao W, Gilmore JH, Shen D, Smith JK, Zhu H, Lin W. The synchronization within and interaction
1001 between the default and dorsal attention networks in early infancy. *Cereb Cortex*. 2013;23(3):594-603.
- 1002 47. Rubinov M, Sporns O. Complex network measures of brain connectivity: uses and
1003 interpretations. *Neuroimage*. Sep 2010;52(3):1059-69. doi:10.1016/j.neuroimage.2009.10.003
- 1004 48. Bullmore E, Sporns O. The economy of brain network organization. *Nat Rev Neurosci*. May
1005 2012;13(5):336-49. doi:10.1038/nrn3214
- 1006 49. Meunier D, Lambiotte R, Bullmore ET. Modular and hierarchically modular organization of brain
1007 networks. *Frontiers in neuroscience*. 2010;4:200. doi:10.3389/fnins.2010.00200

- 1008 50. Uehara T, Tobimatsu S, Kan S, Miyauchi S. Modular organization of intrinsic brain networks: A
1009 graph theoretical analysis of resting-state fMRI. *IEEE*; 2012:722-727.
- 1010 51. Blondel VD, Guillaume J-L, Lambiotte R, Lefebvre E. Fast unfolding of communities in large
1011 networks. *Journal of Statistical Mechanics: Theory and Experiment*. 2008;2008(10):P10008.
- 1012 52. Bassett DS, Bullmore E. Small-world brain networks. *The neuroscientist*. 2006;12(6):512-523.
- 1013 53. Telesford QK, Joyce KE, Hayasaka S, Burdette JH, Laurienti PJ. The ubiquity of small-world
1014 networks. *Brain connectivity*. 2011;1(5):367-375.
- 1015 54. Humphries MD, Gurney K. Network 'small-world-ness': a quantitative method for determining
1016 canonical network equivalence. *PLoS one*. 2008;3(4):e0002051. doi:10.1371/journal.pone.0002051
- 1017 55. Barkovich AJ, Raybaud C. *Pediatric neuroimaging*. Lippincott Williams & Wilkins; 2012.
- 1018 56. Blustajn J, Kirsch C, Panigrahy A, Netchine I. Olfactory anomalies in CHARGE syndrome: imaging
1019 findings of a potential major diagnostic criterion. *Am J Neuroradiol*. 2008;29(7):1266-1269.
- 1020 57. Sato N, Hatakeyama S, Shimizu N, Hikima A, Aoki J, Endo K. MR evaluation of the hippocampus
1021 in patients with congenital malformations of the brain. *Am J Neuroradiol*. 2001;22(2):389-393.
- 1022 58. Righini A, Zirpoli S, Parazzini C, et al. Hippocampal infolding angle changes during brain
1023 development assessed by prenatal MR imaging. *Am J Neuroradiol*. 2006;27(10):2093-2097.
- 1024 59. Montenegro M, Kinay D, Cendes F, et al. Patterns of hippocampal abnormalities in
1025 malformations of cortical development. *Journal of neurology, neurosurgery & psychiatry*.
1026 2006;77(3):367-371.
- 1027 60. Bajic D, Wang C, Kumlien E, et al. Incomplete inversion of the hippocampus—a common
1028 developmental anomaly. *European radiology*. 2008;18(1):138-142.
- 1029 61. Bajic D, Moreira NC, Wikström J, Raininko R. Asymmetric development of the hippocampal
1030 region is common: a fetal MR imaging study. *Am J Neuroradiol*. 2012;33(3):513-518.
- 1031 62. Barkovich AJ, Millen KJ, Dobyns WB. A developmental and genetic classification for midbrain-
1032 hindbrain malformations. *Brain : a journal of neurology*. 2009;132(12):3199-3230.
- 1033 63. Hetts SW, Sherr EH, Chao S, Gobuty S, Barkovich AJ. Anomalies of the corpus callosum: an MR
1034 analysis of the phenotypic spectrum of associated malformations. *Am J Roentgenol*. 2006;187(5):1343-
1035 1348.
- 1036 64. Fernandez-Miranda JC, Pathak S, Engh J, et al. High-definition fiber tractography of the human
1037 brain: neuroanatomical validation and neurosurgical applications. *Neurosurgery*. 2012;71(2):430-453.
- 1038 65. Meyers BD, Lee VK, Dennis LG, et al. Harmonization of Multi-Center Diffusion Tensor
1039 Tractography in Neonates with Congenital Heart Disease: Optimizing Post-Processing and Application of
1040 ComBat. *medRxiv*. 2021;
- 1041 66. Smith SM, Jenkinson M, Johansen-Berg H, et al. Tract-based spatial statistics: voxelwise analysis
1042 of multi-subject diffusion data. *Neuroimage*. 2006;31(4):1487-1505.
- 1043 67. Bellinger DC, Bernstein JH, Kirkwood MW, et al. Visual-spatial skills in children after open-heart
1044 surgery. *Journal of developmental and behavioral pediatrics : JDBP*. 2003;24(3):169--79.
- 1045 68. Bellinger DC, Jonas RA, Rappaport LA, et al. Developmental and neurologic status of children
1046 after heart surgery with hypothermic circulatory arrest or low-flow cardiopulmonary bypass. *N Engl J*
1047 *Med*. Mar 2 1995;332(9):549-55. doi:10.1056/nejm199503023320901
- 1048 69. Bellinger DC, Wypij D, Rivkin MJ, et al. Adolescents with d-transposition of the great arteries
1049 corrected with the arterial switch procedure: neuropsychological assessment and structural brain
1050 imaging. *Circulation*. Sep 20 2011;124(12):1361-9. doi:10.1161/circulationaha.111.026963
- 1051 70. McQuillen PS, Goff DA, Licht DJ. Effects of congenital heart disease on brain development.
1052 *Progress in pediatric cardiology*. 2010;29(2):79--85. doi:10.1016/j.ppedcard.2010.06.011
- 1053 71. Zahid M, Bais A, Tian X, et al. Airway ciliary dysfunction and respiratory symptoms in patients
1054 with transposition of the great arteries. *PLoS one*. 2018;13(2):e0191605.

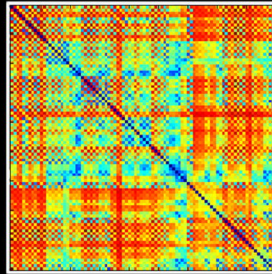
- 1055 72. Li Y, Klena NT, Gabriel GC, et al. Global genetic analysis in mice unveils central role for cilia in
1056 congenital heart disease. *Nature*. 2015;
- 1057 73. Marelli A, Miller SP, Marino BS, Jefferson AL, Newburger JW. Brain in congenital heart disease
1058 across the lifespan: the cumulative burden of injury. *Circulation*. 2016;133(20):1951-1962.
- 1059 74. Wernovsky G, Licht DJ. Neurodevelopmental outcomes in children with congenital heart
1060 disease—what can we impact? *Pediatric critical care medicine: a journal of the Society of Critical Care
1061 Medicine and the World Federation of Pediatric Intensive and Critical Care Societies*. 2016;17(8 Suppl
1062 1):S232.
- 1063 75. Volpe JJ. Encephalopathy of Congenital Heart Disease—Destructive and Developmental Effects
1064 Intertwined. *J Pediatr*. May 2014;164(5):962-5. doi:10.1016/j.jpeds.2014.01.002
- 1065 76. Panigrahy A, Schmithorst VJ, Wisnowski JL, et al. Relationship of white matter network topology
1066 and cognitive outcome in adolescents with d-transposition of the great arteries. *NeuroImage: Clinical*.
1067 2015;7:438-448.
- 1068 77. Mahle WT, Clancy RR, Moss EM, Gerdes M, Jobes DR, Wernovsky G. Neurodevelopmental
1069 outcome and lifestyle assessment in school-aged and adolescent children with hypoplastic left heart
1070 syndrome. *Pediatrics*. May 2000;105(5):1082-9.
- 1071 78. Tabbutt S, Nord AS, Jarvik GP, et al. Neurodevelopmental outcomes after staged palliation for
1072 hypoplastic left heart syndrome. *Pediatrics*. Mar 2008;121(3):476-83. doi:10.1542/peds.2007-1282
- 1073 79. Sananes R, Goldberg CS, Newburger JW, et al. Six-year neurodevelopmental outcomes for
1074 children with single-ventricle physiology. *Pediatrics*. 2021;147(2)
- 1075 80. De Asis-Cruz J, Donofrio MT, Vezina G, Limperopoulos C. Aberrant brain functional connectivity
1076 in newborns with congenital heart disease before cardiac surgery. *NeuroImage: Clinical*. 2017;
- 1077 81. Schiller RM, van den Bosch GE, Muetzel RL, et al. Neonatal critical illness and development:
1078 white matter and hippocampus alterations in school-age neonatal extracorporeal membrane
1079 oxygenation survivors. *developmental medicine & child Neurology*. 2017;59(3):304-310.
- 1080 82. Stinnett GR, Lin S, Korotcov AV, et al. Microstructural Alterations and Oligodendrocyte
1081 Dysmaturation in White Matter After Cardiopulmonary Bypass in a Juvenile Porcine Model. *Journal of
1082 the American Heart Association*. 2017;6(8):e005997.
- 1083 83. Harbison AL, Votava-Smith JK, del Castillo S, et al. Clinical Factors Associated with Cerebral
1084 Metabolism in Term Neonates with Congenital Heart Disease. *The Journal of pediatrics*. 2017;
- 1085 84. Morton PD, Korotcova L, Lewis BK, et al. Abnormal neurogenesis and cortical growth in
1086 congenital heart disease. *Science translational medicine*. 2017;9(374):eaah7029.
- 1087 85. Schmithorst VJ, Panigrahy A, Gaynor JW, et al. Organizational topology of brain and its
1088 relationship to ADHD in adolescents with d-transposition of the great arteries. *Brain and behavior*.
1089 2016;6(8)
- 1090 86. Lim JM, Porayette P, Marini D, et al. Associations between age at arterial switch operation, brain
1091 growth, and development in infants with transposition of the great arteries. *Circulation*.
1092 2019;139(24):2728-2738.



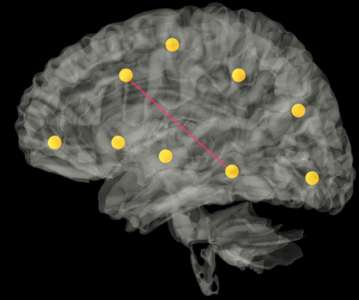
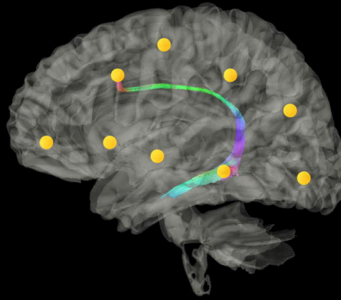
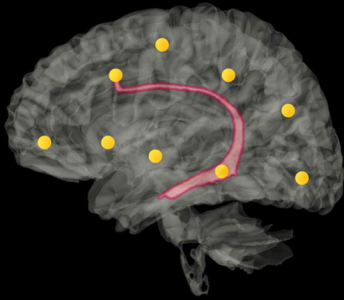
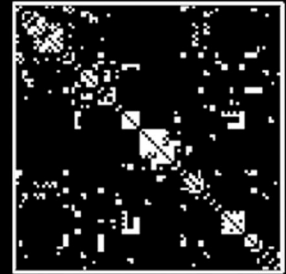
Average FA
Connectome

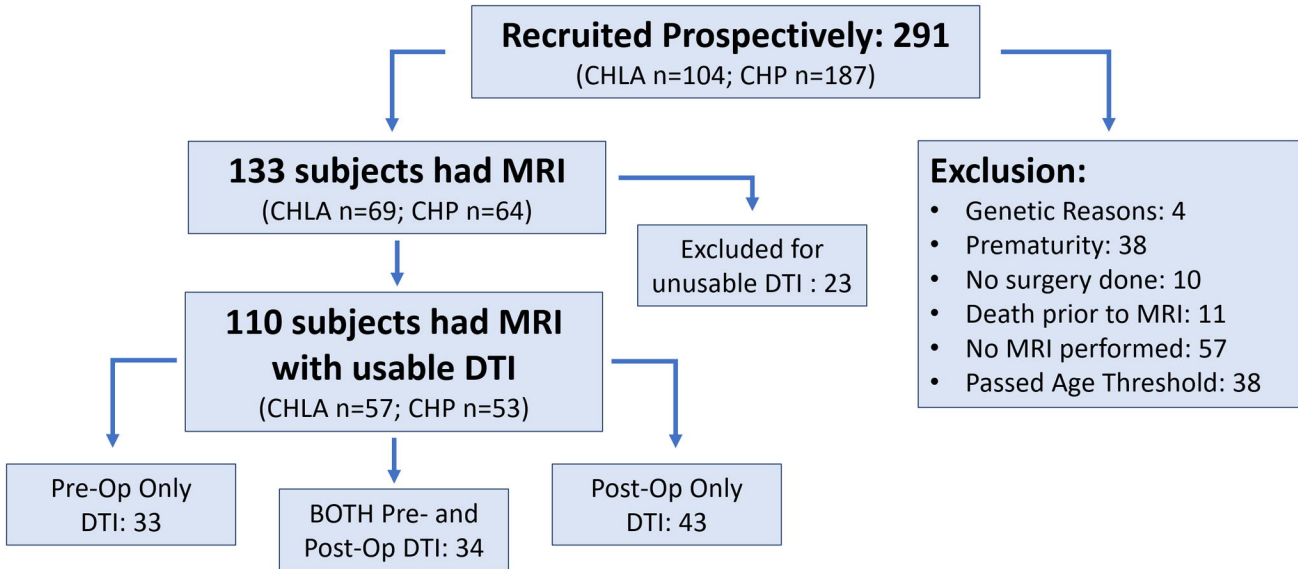


Number of Tracts
Connectome



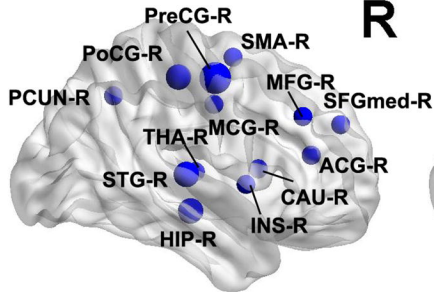
Adjacency
Connectome



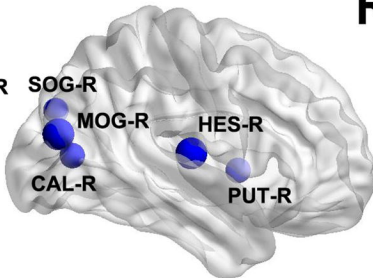


NODAL EFFICIENCY

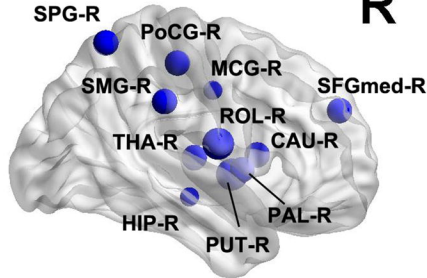
R



R



R



SEVERITY OF FETAL CEREBRAL
SUBSTRATE DELIVERY
pre-operative MR scan

SEIZURES

post-operative MR scan

ECMO

post-operative MR scan

● < 0.05

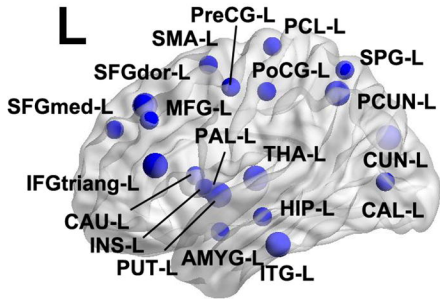
● < 0.01

● < 0.001

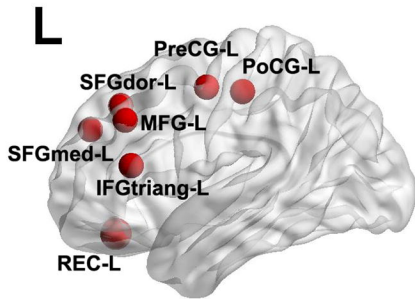
● < 0.0001

● = Decreased

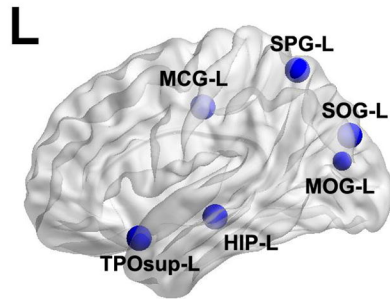
NODAL EFFICIENCY



Hippocampal
Hypoplasia/Dysplasia



Cerebellar
Hypoplasia/Dysplasia



Olfactory
Hypoplasia/Dysplasia

